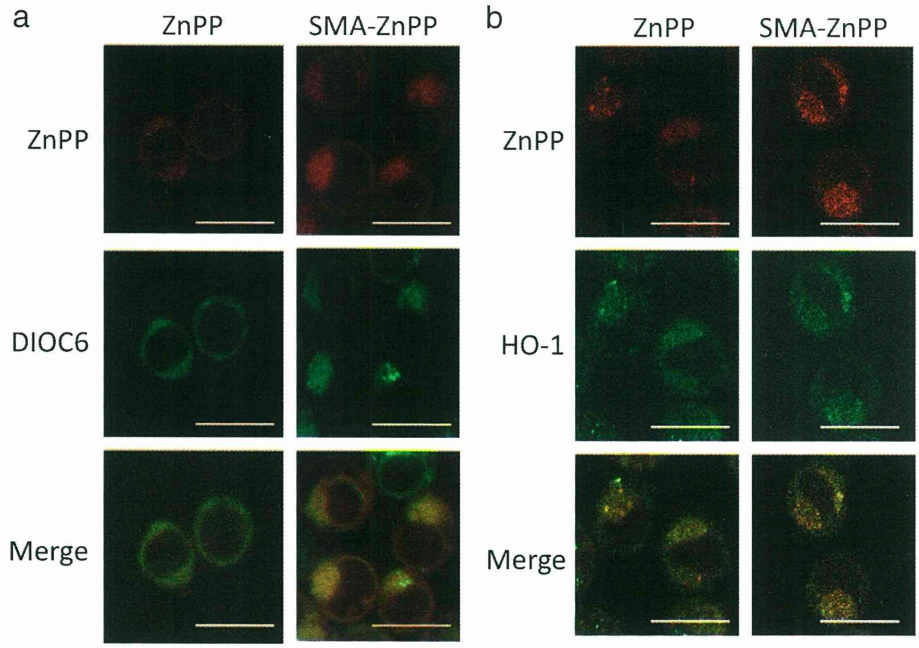

Fig. 5. Subcellular localization of ZnPP micelles. (a) shows the ER localization of ZnPP micelles. ZnPP micelles (red) and DIOC6 (green) were visualized by confocal laser microscopy. (b) shows the colocalization of ZnPP micelles (red) with HO-1 (green). Cells were grown to logarithmic phase, incubated with 30 μM of ZnPP and SMA-ZnPP for 2 h. ER was stained by DIOC6 and HO-1 was visualized with FITC-conjugated to anti-rabbit IgG. Scale bar shows 20 μm in length.

3.5. Liberation of free ZnPP from PEG-ZnPP

As shown in Fig. 1, in the PEG-ZnPP, two PEG chains are covalently linked to the spacer ethylenediamine that is conjugated to the carboxyl group of protoporphyrin IX. ZnPP is a competitive inhibitor of HO-1 thus PEG-cleavage might be critical step to exert HO-1 inhibitory activity. We next examined the intracellular processing of PEG-ZnPP by HPLC analyses. K562 cells were treated with PEG-ZnPP for 5 h at 37 °C in RPMI medium and intracellular PEG-ZnPP or its hydrolysed products was extracted by ethanol followed by HPLC analyses. As shown in Fig. 9, parental PEG-ZnPP had a retention time at 6.3 min and intracellular PEG-ZnPP after incubation with cells and extraction showed delayed

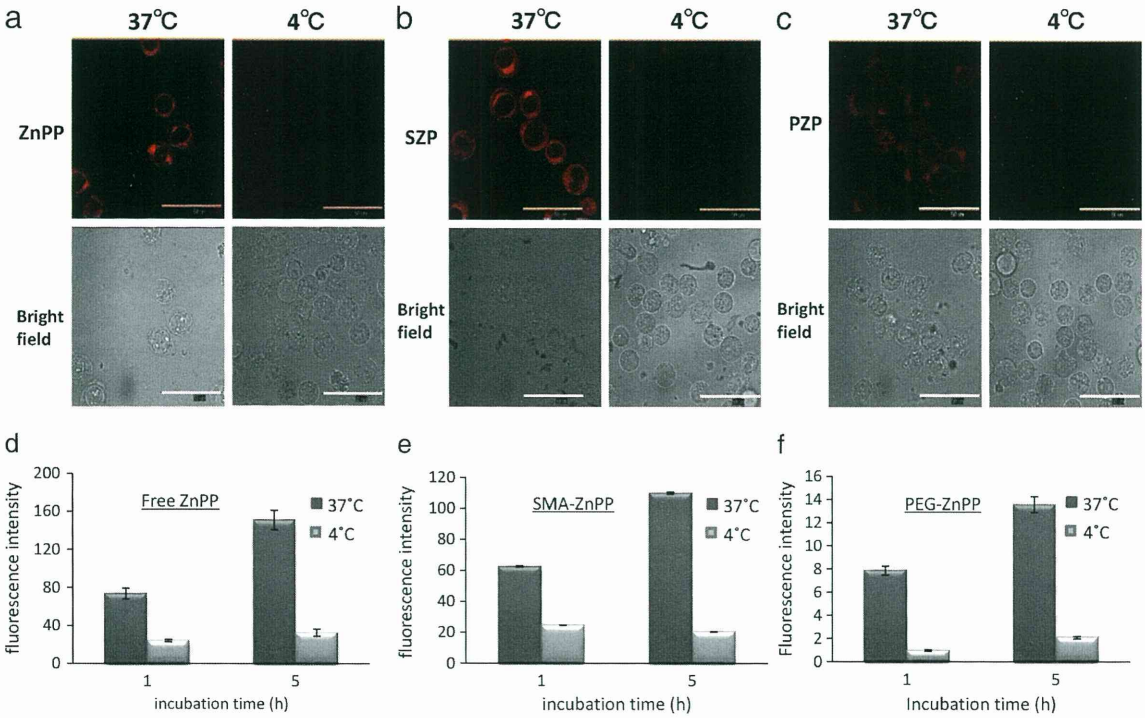

Fig. 6. Intracellular uptake of ZnPP micelles at different temperature. Intracellular ZnPP (red) in K562 cells treated with 20 μM of (a) ZnPP, (b) SMA-ZnPP and (c) PEG-ZnPP for 2 h at 37 °C (left panel) and at 4 °C (right panel) were visualized by confocal laser microscopy. Amount of ZnPP in K562 cells treated with (d) ZnPP, (e) SMA-ZnPP and (f) PEG-ZnPP were quantified by FACS analysis.

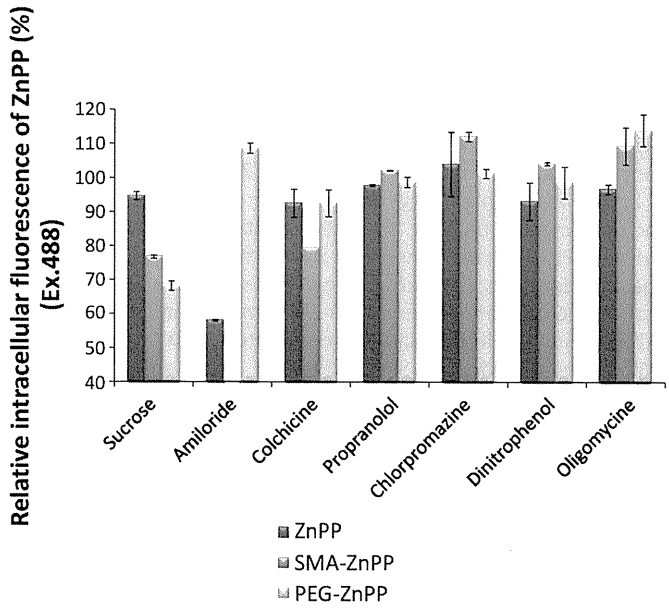

Fig. 7. Inhibition of intracellular uptake of ZnPP micelles by endocytosis inhibitors. K562 cells were treated with ZnPP (black column), SMA-ZnPP (gray column) and PEG-ZnPP (white column) with or without indicated endocytosis inhibitors. Cells were preincubated with these inhibitors for 60 min prior to addition of ZnPP micelles. Intracellular amount of ZnPP was quantified by FACS analysis.

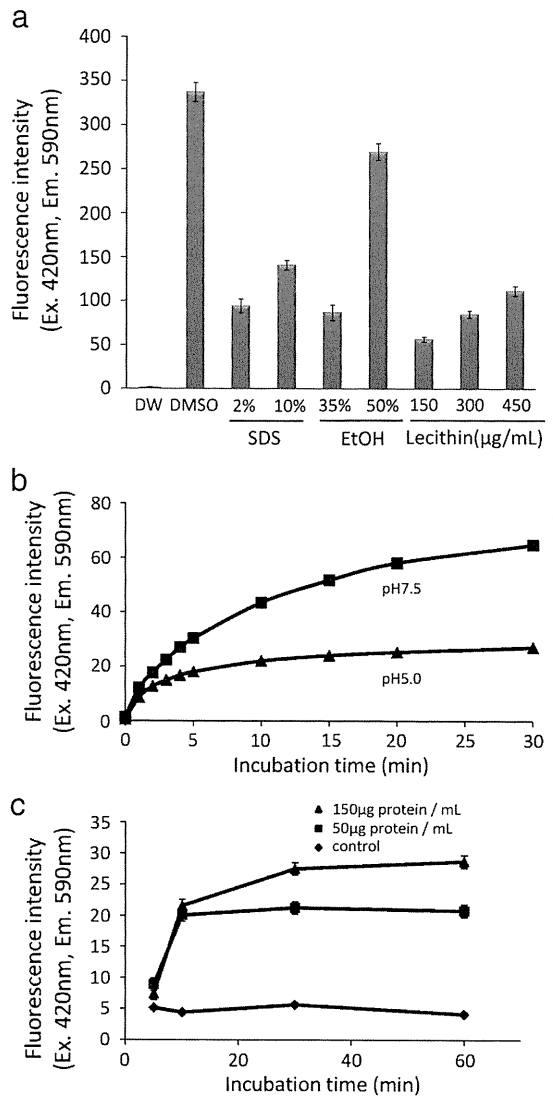

Fig. 8. Stability analysis of SMA-ZnPP and effect of various amphiphilic agents for bursting of micelles. (a) Fluorescence intensity of SMA-ZnPP incubated with different concentration of lecithin for 30 min or SDS for 15 min was measured by fluorescent spectroscopy. (b) Fluorescence intensity of SMA-ZnPP was measured as the micelles were incubated with lecithin at pH 7.5 (square) or pH 5.5 (triangle). (c) Fluorescence intensity of SMA-ZnPP incubated with 150 μg/ml (triangle) and 50 μg/ml (square) of mouse liver microsomal fraction for indicated time.

retention time at 7.1 min indicating the processing of PEG-ZnPP in cells or cell periphery (Fig. 9a). Furthermore this cleaved PEG-ZnPP was also found to have HO-1 inhibitory activity (Fig. 9b).

4. Discussion

The most important properties for anticancer drugs are summerized as follows; (i) selective accumulation of the drugs in the tumor tissue, (ii) efficient intracellular uptake, and (iii) access of active component to the intracellular target molecules. To confer these properties to the candidate drugs, a numbers of methods may be possible. One of the most universal tumor selective targeting is based on the EPR (enhanced permeability and retention) mechanism dependent selective targeting, in which macromolecular formulations are preferred. The first such example is the conjugation of SMA and proteinaceous drug neocarzinostatin (NCS) resulting SMANCS [15,26–28]. For this purpose, encapsulation of the low molecular weight drugs into the micelles or liposome, or conjugation to polymeric carriers such as SMA, HPMA (N-(2-hydroxypropyl)methacrylamide), PEG or other block copolymers with biocompatible and carrier properties. These methods can improve the physicochemical and pharmacokinetic properties of low MW drugs, or various proteins [15,18,29–31].

Both PEG-ZnPP and SMA-ZnPP exhibit micellar property and have molecular weight of about 140 kDa and 90 kDa respectively and mean size distribution about 180 nm and 50 nm respectively. Both PEG-ZnPP and SMA-ZnPP showed high water solubility and accumulate more selectively in the tumor tissue, and they exert potent anti-tumor activity when injected i.v. [8,11].

Although we have characterized in vivo body distribution and anti-tumor effect of both PEG-ZnPP and SMA-ZnPP, mechanism of cellular uptake and intracellular localization remained to be clarified. For this reason, mechanism of cellular uptake and intracellular fate of these micelles were investigated. Very recently, we have reported that growth or DNA synthesis of human chronic myeloid leukemia (CML) derived cell line K562 cells were suppressd by PEG-ZnPP and SMA-ZnPP [7]. In the present study, we report that both PEG-ZnPP and SMA-ZnPP were internalized in K562 cells at different rate. Fluorescent intensity of ZnPP derivatives is highly dependent on its conformational states, π–π stacked form or dispersed free form. Compact molecular packing of ZnPP in SMA micelles quenched fluorescence perhaps by π–π stacking or energy transfer (Figs. 3a and 8). Thus it may be difficult to compare among the intracellular amounts of three ZnPP derivatives by fluorescent intensity such as flowcytometry due to possible quenching (Fig. 6). In the organic solvent such as ethanol, in which ZnPP derivatives are dispersed states, three ZnPP derivatives showed comparable fluorescent intensity (Fig. 3a). This result indicates that fluorescent intensity in ethanol correlates with ZnPP amount of the ZnPP derivatives. Thus we extracted intracellular ZnPP derivatives in ethanol to represent the realistic amount of ZnPP, SMA-ZnPP and PEG-ZnPP in cells. SMA-ZnPP is about 2.5 times more rapidly internalized into the cells than PEG-ZnPP at 300 min (Fig. 3). Increment of uptake when compared from 30 min to 300 min of SMA-ZnPP is 5 times more than PEG-ZnPP (Fig. 3). FACS analysis also supports the faster uptake of SMA-ZnPP; intracellular fluorescent intensity of SMA-ZnPP was 7 times higher than that of PEG-ZnPP at 5 h (Fig. 6). This suppressed uptake of

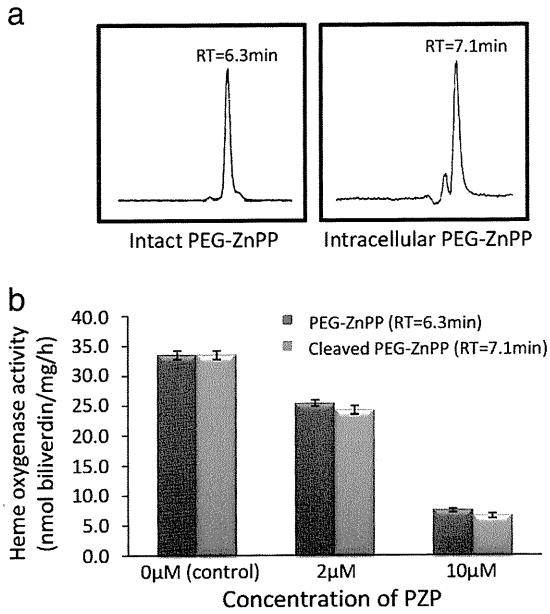

Fig. 9. Intracellular processing of PEG-ZnPP. (a) Shows HPLC analysis of intact PEG-ZnPP (left panel), PEG-ZnPP (right panel). (b) Shows HO-1 inhibitory activity of intact PEG-ZnPP (black column) and cleaved PEG-ZnPP (gray column). Both PEG-ZnPP were preincubated with mouse liver cytosol and spleen microsome for 30 min at 25 °C prior to addition of hemin as a substrate of HO-1 enzyme reaction. HO-1 activity was measured as described in the text.

PEG-ZnPP may be caused by the fact that hydrated PEG-layer of the PEG micelles interferes the interaction with receptor site on the cell surface that is involved in endocytotic uptake of micelles. This suppressed intracellular uptake is named PEG-dilemma [32,33]. Meanwhile, intracellular uptake of SMA-ZnPP was very active and almost comparable to that of free ZnPP. This may be due to the affinity between the hydrophobic residue of SMA and surface receptor. Free ZnPP is internalized most rapidly among the three tested ZnPP derivatives. Nevertheless free ZnPP is poorly water soluble and thus difficult for clinical application, and more important, as small molecule it may disappear from the circulation so rapidly that it never shows EPR effect for tumor delivery. Namely, PEG and SMA based micelle formulation gives high water solubility and improved pharmacokinetic property including high plasma concentration and antitumor activity of ZnPP. However, PEG-ZnPP showed much less efficient cell uptake. As a result PEG-ZnPP exhibited less cytotoxic activity in the in vitro setting compared to free ZnPP or SMA-ZnPP (data not shown). Whereas SMA micelles confer the micellar capacity for efficient cell uptake as reported for SMANCS [34,35].

Cell membrane forms a barrier impermeable to large molecules above about 1 kDa. However, cells are equipped with active transport systems across the cell membrane called endocytosis for most macromolecules such as micelles, liposomes, antibody and DNA/RNA complex. Endocytotic cellular uptake is believed to be more active in dividing cells such as tumor cells than non-dividing normal cells. Previously, SMANCS was shown to undergo endocytotic pathway for its antitumor activity. Namely SMANCS is rapidly internalized into the cells [34,35]. Many other macromolecular drugs such as liposomes and HPMA conjugated drugs also show endocytotic cellular internalization [20–22].

In this study we showed that free ZnPP, SMA-ZnPP micelle and PEG-ZnPP conjugate were internalized by endocytotic pathway. It is considered that at low temperature (below 20 °C), endocytotic uptake of macromolecules was suppressed probably due to suppressed ATP generation by oxidative phosphorylation. Thus suppressed internalization at low temperature (4 °C) and rapid uptake at 37 °C indicate that endocytosis is the major mechanism of cellular drug uptake (Fig. 6). In addition, it should be noted that in this study, the fluorescent intensity of ZnPP, SMA-ZnPP and PEG-ZnPP is directly detected by flowcytometry, not through ethanol extraction method, because of the difference of fluorescent efficiency of ZnPP and derivatives as discussed above, it is difficult to compare the internalized amount of SMA-ZnPP and PEG-ZnPP. Intracellular uptake of ZnPP was significantly inhibited by amiloride, which is a macropinocytosis inhibitor, suggesting that the cellular internalization of ZnPP is partially mediated by macropinocytotic pathway, a type of endocytosis. Cellular uptake of PEG-ZnPP was suppressed by sucrose, and cellular uptake of SMA-ZnPP was suppressed by sucrose and colchicine. Unfortunately precipitates were formed when amiloride was added to SMA-ZnPP that made analysis difficult. These results suggest that PEG-ZnPP is internalized by clathrin dependent endocytosis, whereas SMA-ZnPP is internalized not only by clathrin dependent endocytosis but also probably via microtubule dependent endocytosis mechanism. It seems that several different pathways may be involved in internalization of ZnPP, SMA-ZnPP and PEG-ZnPP. Further investigations are needed to clarify this point.

Protoporphyrin IX (PP) itself doesn't have HO-1 inhibitory effect or cytotoxicity as previously shown. However, ZnPP and both ZnPP micelles were shown to inhibit HO-1 in the cell [8,9], and cells treated with ZnPP and both ZnPP micelles showed the fluorescence spectrum corresponding to free ZnPP, the zinc coordinated form of protoporphyrin IX. This result suggests that after the internalization, both ZnPP micelles still exist as zinc in the tetrapyrrole, an active HO-1 inhibition form of Zn-protoporphyrin IX.

Fluorescence microscopy under a confocal laser microscope, based on the fluorescence of ZnPP was carried out in this study. As shown in Fig. 8, SMA-ZnPP micelle was shown to exhibit less fluorescence compared with free ZnPP in test tube as it was expected so because the fluorescence of SMA-ZnPP was quenched due to π–π interaction in the packed micelle. However, we found fluorescence of ZnPP micelles appeared eventually in the cells, indicating free ZnPP was released from the micelle to exhibit fluorescence. Namely, these results suggested that unique fate of SMA-ZnPP micelles being uncoated in the cells. Moreover as shown in Fig. 4a and b, fluorescence by SMA-ZnPP was found at cellular membrane as well as ER compartment after treatment for first 15 min–120 min. In contrast, PEG-ZnPP (Fig. 4c) showed very weak fluorescence at the ER compartment after the same time. HO-1 was also localized at the ER, colocalization with the fluorescence of ZnPP (see Fig. 5 merge). These results are consistent with an interpretation that ZnPP micelles exert cytotoxic activity through inhibiting to the HO-1 enzyme as free ZnPP.

ZnPP is thought to be tightly packed in the center core of SMA-ZnPP micelles (Fig. 1) as judged by quenching of its fluorescence and emergence of fluorescence upon disruption of the micelles (Fig. 2), suggesting that the liberation of free ZnPP from SMA-ZnPP micelle is needed to exert HO-1 inhibitory activity. Recently, Regehly et al. reported that SMA-ZnPP micelles exist as a free ZnPP-form in the cells and seem to be associated with hydrophobic environment such as lipid bilayer of cellular compartment, the data based on flash photolysis measurement of singlet oxygen [36]. Consistent with this previous report, release of free ZnPP may be brought about by micelle disintegration in the cells caused by the amphiphilic components in cells, particularly cell membrane such as phosphatidyl choline. We therefore examined this process of the ZnPP release in vitro from its SMA-ZnPP micelle with lecithin and microsomal membrane fraction, which was obtained from the tissue homogenate followed by ultracentrifugation at 100,000 g ppt (precipitate). Release of ZnPP was more rapid at pH 7.5 than pH 5.5. These observations suggest that disruption of SMA-ZnPP micelles proceeds in the presence of membrane component of cells as well as binding to lipophilic compartments in the cell such as ER compartment.

Recently Huan et al. synthesized PEG-lipid derivatives linked via ester linkage, ether linkage and amide linkage respectively. They

showed that PEG-lipid linked via ester linkage is most susceptible to PEG cleavage [37]. We also confirmed that PEG-ZnPP linked via ether linkage was more stable than PEG-ZnPP conjugated via ester linkage, and cleavage of ester linkage was accelerated by serum component (unpublished data). Along this line we clarified that PEG-ZnPP containing ester linkage is cleaved intracellularly (Fig. 9a). These findings suggest that ester linkage between PEG and ZnPP is the cleavable site by enzyme dependent or independent hydrolytic mechanisms (Fig. 1a). After cleavage of PEG-ZnPP still have HO-1 inhibition activity (Fig. 9b).

In conclusion, we demonstrated here the uptake of different micelle preparations of ZnPP and their fate in the cells. SMA-ZnPP is internalized into cells much more rapidly than PEG-ZnPP by endocytotic pathway, followed by release of free ZnPP in the presence of membrane components. ZnPP is mainly colocalized with HO-1 at ER compartment and inhibits HO-1 activity which leads to higher oxystress then cell death. PEG-ZnPP is also internalized in cells slowly by endocytotic pathway and subjected of hydrolytic cleavage by either protease or esterase inside of, or in the vicinity of, the cells. PEG-ZnPP also shows colocalization with HO-1 and inhibits the HO-1 activity perhaps after the cleavage of PEG bond.

References

[1] S. Ishizawa, T. Yoshida, G. Kikuchi, Induction of heme oxygenase in rat liver. Increase of the specific mRNA by treatment with various chemicals and immunological identity of the enzymes in various tissues as well as the induced enzymes, J. Biol. Chem. 258 (7) (1983) 4220–4225.

[2] R.K. Kutty, M.D. Maines, Effects of induction of heme oxygenase by cobalt and tin on the in vivo degradation of myoglobin, Biochem. Pharmacol. 33 (18) (1984) 2924–2926.

[3] T.J. Smith, S. Haque, G.S. Drummond, Induction of heme oxygenase mRNA by cobalt protoporphyrin in rat liver, Biochim. Biophys. Acta 1073 (1) (1991) 221–224.

[4] K. Doi, T. Akaike, S. Fujii, S. Tanaka, N. Ikebe, T. Beppu, S. Shibahara, M. Ogawa, H. Maeda, Induction of haem oxygenase-1 nitric oxide and ischaemia in experimental solid tumours and implications for tumour growth, Br. J. Cancer 80 (12) (1999) 1945–1954.

[5] J.H. Kaplan, J.N. Groves, Liver and blood cell catalase activity of tumor-bearing mice, Cancer Res. 32 (6) (1972) 1190–1194.

[6] A.M. Tarakhovskii, G.V. Glinskii, V.A. Shliakhovenko, Superoxide dismutase activity in tumor and liver of tumor-bearing animals, Ukr. Biokhim. Zh. 52 (5) (1980) 628–631.

[7] M. Mayerhofer, K.V. Gleixner, J. Mayerhofer, G. Hoermann, E. Jaeger, K.J. Aichberger, R.G. Ott, K. Greish, H. Nakamura, S. Derdak, P. Samorapoompichit, W.F. Pickl, V. Sexl, H. Esterbauer, I. Schwarzinger, C. Sillaber, H. Maeda, P. Valent, Targeting of heat shock protein 32 (Hsp32)/heme oxygenase-1 (HO-1) in leukemic cells in chronic myeloid leukemia: a novel approach to overcome resistance against imatinib, Blood 111 (4) (2008) 2200–2210.

[8] J. Fang, T. Sawa, T. Akaike, T. Akuta, S.K. Sahoo, G. Khaled, A. Hamada, H. Maeda, In vivo antitumor activity of pegylated zinc protoporphyrin: targeted inhibition of heme oxygenase in solid tumor, Cancer Res. 63 (13) (2003) 3567–3574.

[9] S.K. Sahoo, T. Sawa, J. Fang, S. Tanaka, Y. Miyamoto, T. Akaike, H. Maeda, Pegylated zinc protoporphyrin: a water-soluble heme oxygenase inhibitor with tumor-targeting capacity, Bioconjug. Chem. 13 (5) (2002) 1031–1038.

[10] H.W. Hwang, J.R. Lee, K.Y. Chou, C.S. Suen, M.J. Hwang, C. Chen, R.C. Shieh, L.Y. Chau, Oligomerization is crucial for the stability and function of heme oxygenase-1 in the endoplasmic reticulum, J. Biol. Chem. 284 (34) (2009) 22672–22679.

[11] A.K. Iyer, K. Greish, J. Fang, R. Murakami, H. Maeda, High-loading nanosized micelles of copoly(styrene-maleic acid)-zinc protoporphyrin for targeted delivery of a potent heme oxygenase inhibitor, Biomaterials 28 (10) (2007) 1871–1881.

[12] K. Greish, A. Nagamitsu, J. Fang, H. Maeda, Copoly(styrene-maleic acid)-pirarubicin micelles: high tumor-targeting efficiency with little toxicity, Bioconjug. Chem. 16 (1) (2005) 230–236.

[13] J. Fang, T. Sawa, T. Akaike, H. Maeda, Tumor-targeted delivery of polyethylene glycol-conjugated D-amino acid oxidase for antitumor therapy via enzymatic generation of hydrogen peroxide, Cancer Res. 62 (11) (2002) 3138–3143.

[14] J.J. Shiah, Y. Sun, C.M. Peterson, J. Kopecek, Biodistribution of free and N-(2-hydroxypropyl)methacrylamide copolymer-bound mesochlorin e(6) and adriamycin in nude mice bearing human ovarian carcinoma OVCAR-3 xenografts, J. Control. Release 61 (1–2) (1999) 145–157.

[15] Y. Matsumura, H. Maeda, A new concept for macromolecular therapeutics in cancer chemotherapy: mechanism of tumoritropic accumulation of proteins and the antitumor agent smancs, Cancer Res. 46 (12 Pt 1) (1986) 6387–6392.

[16] H. Maeda, T. Sawa, T. Konno, Mechanism of tumor-targeted delivery of macromolecular drugs, including the EPR effect in solid tumor and clinical overview of the prototype polymeric drug SMANCS, J. Control. Release 74 (1–3) (2001) 47–61.

[17] H. Maeda, Nitroglycerin enhances vascular blood flow and drug delivery in hypoxic tumor tissues: analogy between angina pectoris and solid tumors and enhancement of the EPR effect, J Control Release 142 (3) (2010) 296–298.

[18] H. Maeda, G.Y. Bharate, J. Daruwalla, Polymeric drugs for efficient tumor-targeted drug delivery based on EPR-effect, Eur. J. Pharm. Biopharm. 71 (3) (2009) 409–419.

[19] G. Gregoriadis, E.D. Neerunjun, Treatment of tumour bearing mice with liponsome-entrapped actinomycin D prolongs their survival, Res. Commun. Chem. Pathol. Pharmacol. 10 (2) (1975) 351–362.

[20] O. Hovorka, T. Etrych, V. Subr, J. Strohalm, K. Ulbrich, B. Rihova, HPMA based macromolecular therapeutics: internalization, intracellular pathway and cell death depend on the character of covalent bond between the drug and the peptidic spacer and also on spacer composition, J. Drug Target. 14 (6) (2006) 391–403.

[21] K. Sasaki, K. Kogure, S. Chaki, Y. Kihira, M. Ueno, H. Harashima, Construction of a multifunctional envelope-type nano device by a SUV*-fusion method, Int. J. Pharm. 296 (1–2) (2005) 142–150.

[22] C. Allen, Y. Yu, A. Eisenberg, D. Maysinger, Cellular internalization of PCL(20)-b-PEO (44) block copolymer micelles, Biochim. Biophys. Acta 1421 (1) (1999) 32–38.

[23] P. Lemieux, M. Page, C. Noel, In vivo cytotoxicity and antineoplastic activity of a transferrin-daunorubicin conjugate, In Vivo 6 (6) (1992) 621–627.

[24] P. van der Sluijs, H.P. Bootsma, B. Postema, F. Moolenaar, D.K. Meijer, Drug targeting to the liver with lactosylated albumins: does the glycoprotein target the drug or is the drug targeting the glycoprotein? Hepatology 6 (4) (1986) 723–728.

[25] C.P. Leamon, I. Pastan, P.S. Low, Cytotoxicity of folate-Pseudomonas exotoxin conjugates toward tumor cells. Contribution of translocation domain, J. Biol. Chem. 268 (33) (1993) 24847–24854.

[26] G.T. Colbern, D.J. Dykes, C. Engbers, R. Musterer, A. Hiller, E. Pegg, R. Saville, S. Weng, M. Luzzio, P. Uster, M. Amantea, P.K. Working, Encapsulation of the topoisomerase I inhibitor GL147211C in pegylated (STEALTH) liposomes: pharmacokinetics and antitumor activity in HT29 colon tumor xenografts, Clin. Cancer Res. 4 (12) (1998) 3077–3082.

[27] Y. Matsumura, T. Oda, H. Maeda, General mechanism of intratumor accumulation of macromolecules: advantage of macromolecular therapeutics, Gan To Kagaku Ryoho. 14 (3 Pt 2) (1987) 821–829.

[28] H. Maeda, J. Takeshita, R. Kanamaru, A lipophilic derivative of neocarzinostatin. A polymer conjugation of an antitumor protein antibiotic, Int. J. Pept. Protein Res. 14 (2) (1979) 81–87.

[29] K.A. Nieforth, R. Nadeau, I.H. Patel, D. Mould, Use of an indirect pharmacodynamic stimulation model of MX protein induction to compare in vivo activity of interferon alfa-2a and a polyethylene glycol-modified derivative in healthy subjects, Clin. Pharmacol. Ther. 59 (6) (1996) 636–646.

[30] T.M. Allen, C. Hansen, F. Martin, C. Redemann, A. Yau-Young, Liposomes containing synthetic lipid derivatives of poly(ethylene glycol) show prolonged circulation half-lives in vivo, Biochim. Biophys. Acta 1066 (1) (1991) 29–36.

[31] H. Maeda, Tumor-selective delivery of macromolecular drugs via the EPR effect: background and future prospects. Bioconjug Chem 21(5) 797–802.

[32] T. Masuda, H. Akita, K. Niikura, T. Nishio, M. Ukawa, K. Enoto, R. Danev, K. Nagayama, K. Ijiro, H. Harashima, Envelope-type lipid nanoparticles incorporating a short PEG-lipid conjugate for improved control of intracellular trafficking and transgene transcription, Biomaterials 30 (27) (2009) 4806–4814.

[33] H. Hatakeyama, H. Akita, K. Kogure, M. Oishi, Y. Nagasaki, Y. Kihira, M. Ueno, H. Kobayashi, H. Kikuchi, H. Harashima, Development of a novel systemic gene delivery system for cancer therapy with a tumor-specific cleavable PEG-lipid, Gene Ther. 14 (1) (2007) 68–77.

[34] T. Oda, F. Sato, H. Maeda, Facilitated internalization of neocarzinostatin and its lipophilic polymer conjugate, SMANCS, into cytosol in acidic pH, J Natl Cancer Inst 79 (6) (1987) 1205–1211.

[35] T. Oda, H. Maeda, Binding to and internalization by cultured cells of neocarzinostatin and enhancement of its actions by conjugation with lipophilic styrene-maleic acid copolymer, Cancer Res. 47 (12) (1987) 3206–3211.

[36] M. Regehly, K. Greish, F. Rancan, H. Maeda, F. Bohm, B. Roder, Water-soluble polymer conjugates of ZnPP for photodynamic tumor therapy, Bioconjug. Chem. 18 (2) (2007) 494–499.

[37] H. Xu, Y. Deng, D. Chen, W. Hong, Y. Lu, X. Dong, Esterase-catalyzed dePEGylation of pH-sensitive vesicles modified with cleavable PEG-lipid derivatives, J. Control. Release 130 (3) (2008) 238–245.

Journal of Drug Targeting, 2011; 19(10): 954–966
© 2011 Informa UK, Ltd.
ISSN 1061-186X print/ISSN 1029-2330 online
DOI: 10.3109/1061186X.2011.633260

informa
healthcare

RESEARCH ARTICLE

4-Amino-6-hydroxypyrazolo [3,4-d]pyrimidine (AHPP) conjugated PEG micelles: Water soluble polymeric xanthine oxidase inhibitor

Gahininath Y. Bharate[1,2], Jun Fang[1], Hideaki Nakamura[1], Haibo Qin[1], Seiji Shinkai[2], and Hiroshi Maeda[1,2]

[1]*Drug Delivery System Research Institute, Faculty of Pharmaceutical Sciences, and* [2]*Department of Nanoscience and Applied Chemistry, Graduate School of Engineering, Sojo University, Ikeda, Kumamoto, Japan*

Abstract

Xanthine oxidase (XO) is the major source of superoxide anion ($O_2^{\bullet-}$) that is associated with various reactive oxygen species (ROS) related diseases. 4-amino-6-hydroxypyrazolo[3,4-d]pyrimidine (AHPP) is a potent XO inhibitor discovered in Maeda's laboratory, which is now being developed for the treatment of ischemia reperfusion injury and inflammatory diseases. However, the poor aqueous solubility of AHPP at physiological pH hampers its clinical development. To overcome this drawback, in the present study water soluble polyethyleneglycol conjugated AHPP (AHPP-PEG) was synthesized via two different approaches, which resulted in two derivatives of AHPP-PEG, namely, mono-AHPP-PEG and bis-(AHPP)-PEG depending on the number of AHPP on PEG chain. We characterized both conjugates by UV, FTIR spectroscopy and elemental analysis. Dynamic light scattering and Sephadex G-100 chromatography studies revealed mean particle size of 164.1 and 218.8 nm and Mw. equivalent to 107 and 126 kDa for mono-AHPP-PEG and bis-(AHPP)-PEG, respectively. Further, XO inhibitory activity for mono-AHPP-PEG and bis-(AHPP)-PEG were found with Ki of 0.23 ± 0.03 and 0.21 ± 0.03 μM, respectively. *In vivo* pharmacokinetic study showed longer circulation time of AHPP-PEG conjugates compared to free AHPP. These results indicate AHPP-PEG conjugates have better potentials with supramolecular assemblies in aqueous medium and may become a good candidate for the treatment of ROS related diseases.

Keywords: Pharmacokinetics, superoxide anion, xanthine oxidase, AHPP, inflammation targeted, cytoprotection

Introduction

Xanthine oxidase (XO) is known to exist in many tissues including heart and they catalyses the two-step oxidation of hypoxanthine (Figure 1), from hypoxanthine to xanthine, and then xanthine to uric acid (Cappola et al. 2001; Freehold et al. 1972; Feigelson et al. 1957). XO is well known as a major enzyme to generate superoxide anion ($O_2^{\bullet-}$) that is a major type of reactive oxygen species (ROS) involved in many diseases and disorders, including damaged tissues as well as in the vascular system (Adachi et al. 1993; Jarasch et al. 1981; Jarasch et al. 1986; Oates et al. 2001; Pacher et al. 2006). Moreover, superoxide anion radical ($O_2^{\bullet-}$) immediately reacts with nitric oxide (NO) at diffusion dependent velocity to form more toxic peroxynitrite ($ONOO^-$), which is principally involved in the pathogenesis of various inflammatory disorders including viral and bacterial infections (Oda et al. 1989; Huie et al. 1993; Radi et al. 1991; Crow et al. 1995; Gryglewski et al. 1986; Moncada et al. 1991). In this connection, we previously verified that inhibition of xanthine oxidase resulted in the prolongation of biologic $t_{1/2}$ of NO *in vivo*, which consequently resulted in the lowering of blood pressure.

Thus, inhibiting XO may become a therapeutic to many diseases including inflammation and hypertension. Among inhibitors of XO, allopurinol is used in

Address for Correspondence: Prof. Hiroshi Maeda, Laboratory of Microbiology and Oncology, Faculty of Pharmaceutical Sciences, Sojo University, Ikeda 4-22-1, Kumamoto, 860 0082, Japan. Tel/Fax: +81-96-326-4114. E-mail: hirmaeda@ph.sojo-u.ac.jp

(Received 11 September 2011; revised 15 October 2011; accepted 16 October 2011)

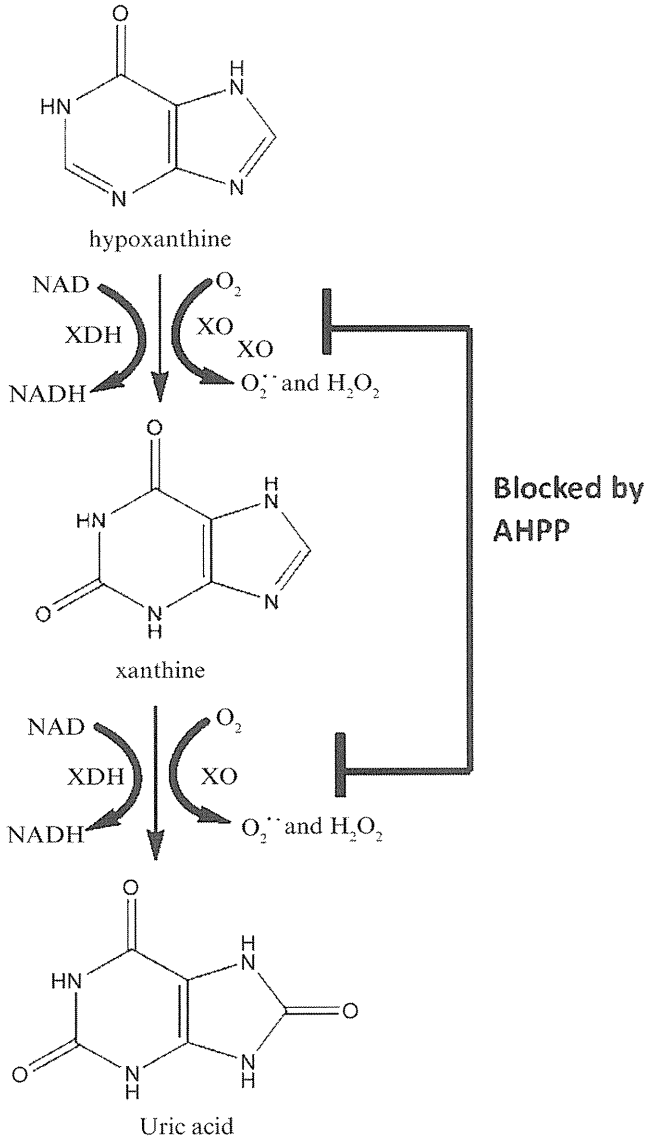

Figure 1. The degradation pathway of purine. XO catalyze the oxidation of hypoxanthine to xanthine and further catalyze the oxidation of xanthine to uric acid. This enzyme plays important role in catabolism of purine. In the reaction of xanthine to uric acid, an oxygen atom is transferred from molyobdenum to xanthine.

clinic for the treatment of hyperuricemia, but the effect of allopurinol is not dose-dependent, at higher dose it becomes substrate of XO (Miyamoto et al. 1996). Recently, we developed 4-amino-6-hydroxypyrazolo [3,4-d] pyrimidine (AHPP), one of the pyrazolopyrimidine derivatives that has exhibited potent XO inhibitory activity. However, AHPP *per se* shows poor aqueous solubility, which prevents clinical development. To overcome this drawback in the current study, we synthesized two water-soluble conjugates of AHPP (4-amino-6-hydroxypyrazolo [3,4-d] pyrimidine) with PEG (polyethyleneglycol).

In addition, the present AHPP-PEG conjugates are designed to exhibit macromolecular nature and thus showed longer plasma half-life and selectively accumulation in inflammatory tissues by taking advantage of the enhanced vascular permeability and retention (EPR) effect (Matsumura et al. 1986; Maeda et al. 2001a, 2001b). Thus, AHPP-PEG conjugates may become a new candidate for ROS related diseases such as inflammatory disease. In this study, the synthesis and characterization of AHPP-PEG were investigated. The *in vivo* pharmacokinetics was also discussed.

Materials and experimental methods

Materials

Poly(oxy-1,-2-ethanediyl)-α-methyl-ω-[2-[(2,5-dioxopyrrolidinyl)oxy]-2-oxoethyoxy]-PEG (Sunbright ME-020AS; Mw 2280; PDI 0.2) was obtained from NOF Corp., Tokyo, Japan. 4-amino-6-hydroxypyrazolo- [3,4-d] pyrimidine (AHPP), xanthine, polyethylene glycol (mean Mn, 2000), 4-phenylspiro[furan-2(3H)-1′-phthalan]-3,3′-dione (fluorescamine), 2,4,6-trinitrobenzenesulfonic acid (TNBS), trichloroacetic acid and other reagents of reagent grade, were purchased from Wako Pure Chemical Industries (Osaka) and were used without further purification. 4-nitrophenyl chloroformate, Bovine milk xanthine oxidase (XO) was purchased from Sigma-Aldrich Chemical Co, (St Louis, MO, USA). AHPP and xanthine solutions were prepared by dissolution in 0.25 M NaOH at a concentration of 0.1 M and were diluted to appropriate concentration with distilled water or physiological saline. All other solvents and chemical reagents were purchased from commercial sources and used without further purification.

Experimental methods

Synthesis of mono-AHPP-PEG conjugated micelles

As depicted in the reaction Scheme 1, 100 mg (0.661 mmol) of 4-amino-6-hydroxypyrazolo [3,4-d] pyrimidine (AHPP) was first dissolved in 15 mL of 0.1 M NaOH solution at room temperature, under stirring for 15 min. Then the solution was cooled to 0–4°C, 1.322 g (0.661 mmol) of poly(oxy-1, 2-ethanediyl)-α-methyl-ω-[2-(2,5-dioxopyrrolidinyl)oxy]-2-oxoethyoxy]-PEG (PEG ME-20AS, NOF Corp.) in 20 mL chloroform was added drop wise for 40 min at 4°C with vigorous stirring. When the addition of PEG was completed the reaction mixture was vigorously stirred for next 2 h at 4°C. The reaction between two components in two layers will undergo as interfacial conjugation reaction under vigorous stirring. Then, the chloroform layer containing the final product (lower layer) was separated by using separating funnel. Chloroform was removed by using a rotary evaporator in vacuum and the conjugate was precipitated by addition with acetone. The resultant viscous product was then dissolved in 40 mL deionized water and lyophilized to obtain fluffy colorless product of mono-AHPP-PEG, conjugate (1.23 g; 87% based on AHPP). By addition of about 50 mL of water to mono-AHPP-PEG, it was readily

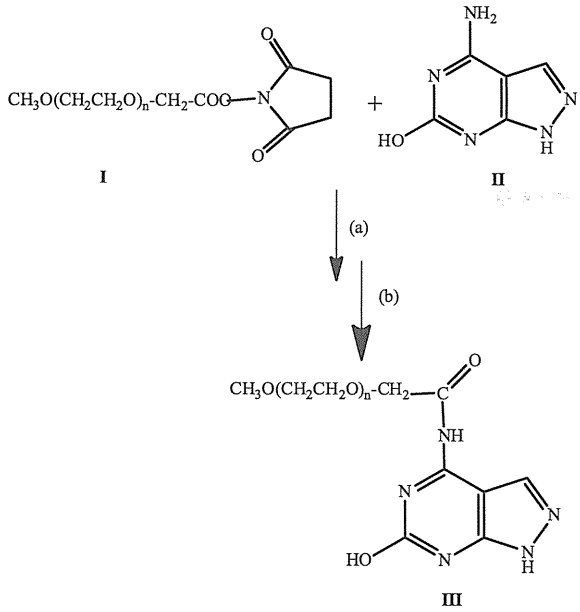

Scheme 1. Synthetic scheme for synthesis of mono-AHPP-PEG conjugate. 0.1 M NaOH, $CHCl_3$, 0°C, pH 9.0; 0.1 M HCl, room temperature, pH 1.5.

solubilized, spontaneously formed micelles. The solution was then subjected to gel chromatography with Sephadex G-100 Fine column (Ø1.5 × 87 cm) (Amersham Biosciences AB, Uppsala, Sweden); Elution peaks corresponding to absorption of AHPP-PEG conjugate at 270 nm was collected, lyophilized and used for further analysis.

Synthesis of bis-(AHPP)-PEG conjugate

As depicted in the reactions Scheme 2, bis-(AHPP)-PEG synthesis was carried out via two-step processes, involving activation of PEG with 4-nitrophenyl chloroformate using a method reported (Varonese et al. 1985; Varonese et al. 2005), followed by interfacial reaction with AHPP. Briefly, to a solution of 5.0 g (2.5 mmol) PEG in 20 mL dry dimethylformamide (DMF), 1.3 g (6.4 mmol) of 4-nitrophenyl chloroformate was added by several aliquots. After stirring this reaction mixture at room temperature for 24 h, 250 mL of dry diethyl ether was added to precipitate the product. The precipitates were then collected by filtration and washed three times with diethyl ether, and the residue was redissolved in acetonitrile:ethylether (1:3 v/v). The product was allowed to precipitate at 4°C for 2 h. Finally, the activated PEG was collected by filtration and dried under vacuum (yield 4.8 g). Further, bis-(AHPP)-PEG was synthesized following the same protocol as used above to synthesis of mono-AHPP-PEG. Yield of bis-(AHPP)-PEG obtained was 1.39 g (91.4%).

Gel filtration chromatography of AHPP-PEG micelles

For purification and characterization of AHPP-PEG micelles, gel chromatography with Sephadex G-100 superfine (Amersham Biosciences AB, Uppsala, Sweden) was performed by using column of Ø1.5 × 87 cm, eluted with 0.1 M bicarbonate pH 8.2. Each eluted 3.1 mL fractions were monitored by UV absorption at 270 nm, and peak fractions were collected followed by dialysis and lyophilized. The lyophilized powder thus obtained was subjected to further characterization by UV-visible and FTIR spectroscopy. To estimate the apparent molecular size of the AHPP-PEG conjugates the size exclusion chromatography was performed using various known molecular weight globular proteins as reference standards.

Dynamic light scattering (DLS)

DLS studies were carried out with a Photal DLS-7000 HLs laser-light scattering spectrophotometer (Otsuka Electronics, Osaka, Japan), equipped with a 10 mW He-Ne (632.5 nm) laser light source. For DLS measurements, the scattering angle was fixed at 90° and the temperature of the sample was maintained at 25.0 ± 0.01°C. Particle size determination was carried out using samples at concentration of 2.5 mg/mL prepared in 0.15 M NaCl/0.01 M sodium phosphate buffer (pH 7.4), which yielded the optimal counts.

UV-visible spectroscopy

UV/visible absorption spectra were recorded on a spectrophotometer (Model UV/Vis-550, JASCO Corp., Tokyo, Japan). The drug concentration was quantified using absorption at 270 nm, based on a standard curve for free AHPP in 0.1 M NaOH (by further diluting 100–10 μM with buffer at pH 8.5).

Fourier transform infrared (FTIR) spectroscopy

Fourier transform infrared (FTIR) spectra were recorded on a FT/IR-4200 spectrometer (JASCO Corp., Tokyo, Japan) using KBr discs. The KBr discs were prepared using Jasco MP-1 minipress unit.

Fluorescence spectroscopy

Fluorescence spectra were recorded on F-2500 fluorescence spectrophotometer (Hitachi, Tokyo). The sample solutions of AHPP and AHPP-PEG conjugates were excited at 270.0 nm (corresponding to λmax of AHPP) and emission for fluorescence from 280.0 to 500.0 nm were measured.

Elemental analysis

Analysis of the AHPP-PEG conjugates after purification by Sephadex column chromatography and drying over P_2O_5 for three days in vacuum were carried out for hydrogen, carbon and nitrogen.

Quantification of amino group after PEGylation by 2,4,6-trinitrobenzendsulfonic acid (TNBS) and fluorescamine assay

The degree of PEG conjugation to AHPP was measured by quantifying the primary amino group by the TNBS (Stocks et al. 1986) with modifications. AHPP, mono-AHPP-PEG and bis-(AHPP)-PEG (for details see Figure 5A) were dissolved in 0.01 M NaOH and further diluted to

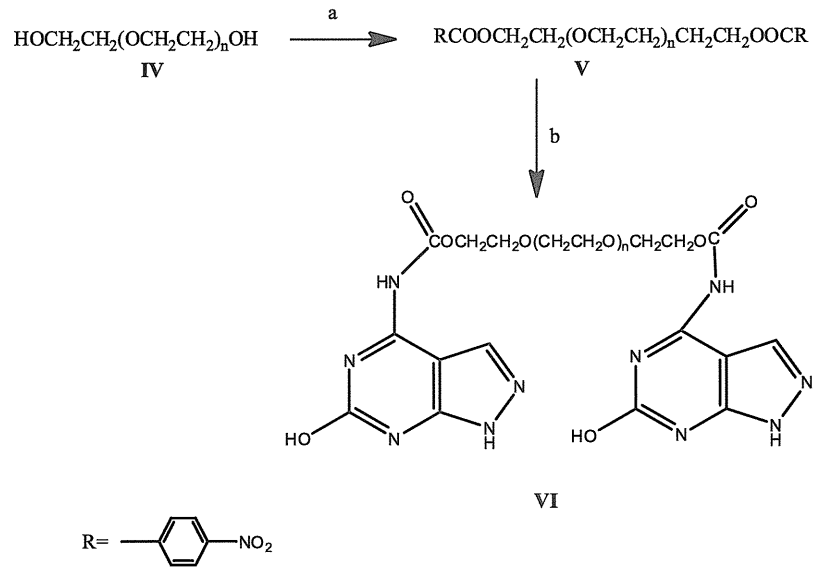

Scheme 2. Synthetic scheme for synthesis of bis-(AHPP)-PEG conjugate. (a) 4-nitrophenyl chloroformate, DMF, 25°C; (b) AHPP, chloroform, 25°C.

final concentrations with 0.1 M borate buffer (pH 8.0). Then, 0.1 mL of 0.1 M TNBS (Wako Pure Chemicals, Osaka) solution was added and vortexed for five minutes. Their absorbances were recorded at 355.0 nm. Moreover, quantification of amino groups was also carried out by use of fluorescamine (4-phenylspiro[furan-2(3H)-1′-phthalan]-3,3′-dione) assay. Briefly, solutions of AHPP and AHPP-PEG conjugates were prepared with a final concentration of 1.0–8.0 μM/mL by serial dilutions using 0.1 M borate buffer (pH 8.0), and 0.5 mL of fluorescamine (Wako Pure Chemicals, Osaka) solution (0.3 mg/mL in acetone) was added. The mixture was vortexed for 2 min and the fluorescence was measured using a florescence spectrophotometer (F-2500, Hitachi High-Technology Corp., Tokyo); excitation at 390.0 nm was used and emission at 475.0 nm was measured.

Release of AHPP-PEG conjugate from its micelle

The release of AHPP-PEG conjugate from the micelles *in vitro* was verified by placing the micellar solutions (2.0 mg in 1.0 mL of 0.2 M phosphate buffer) in sealed dialysis tubes (Mw cut-off 10,000; Spectapor, Spectrum Laboratories, San Diego, CA). The sealed dialysis tubes were submerged in 35.0 mL of (i) pH 6.0 of 0.2 M phosphate buffer; (ii) pH 7.4 of 0.2 M phosphate buffer, and (iii) pH 9.0, 0.2 M carbonate buffers. The dialysis bags were then incubated with reciprocal shaking of the dialysis bath at 1 Hz for several hours at 37°C. The release from the dialysis bags were quantified spectroscopically by measuring absorbance at 270 nm.

Measurement of XO activity and inhibition by AHPP-PEG conjugates

Formation of uric acid from xanthine was measured by absorbance at 290 nm with upon addition of xanthine oxidase (XO). Briefly, AHPP and xanthine were dissolved in 0.1 M NaOH at first, and then diluted with 10 mM sodium phosphate buffer (pH 7.4) final concentration of about 100 μM. Bovine milk XO stock (23 unit /mL, Sigma-Aldrich) was diluted to 330 mU/mL with phosphate buffer (pH 7.4) and further diluted to 1.5 mU/mL. Cuvette containing 1.5 mU/mL of XO (final concentration) in 10 mM sodium phosphate buffer (pH 7.5), graded amounts of xanthine, mono-AHPP-PEG and bis-(AHPP)-PEG, respectively, were added to start the reaction (for details see Figure 8). The velocity of uric acid formation at 25°C was determined as evidenced by the increase in absorbance at 290 nm.

In vivo *pharmacokinetics of AHPP-PEG micelles*

Male ddY mice of 6-week were used in the pharmacokinetics study of AHPP-PEG conjugates. mono-AHPP-PEG and bis-(AHPP)-PEG (dissolved in physiological saline) or free AHPP (dissolved in 0.01 M NaOH) was injected intravenously (i.v.) at 10 mg/kg (AHPP equivalent). After scheduled intervals, mice were killed and blood was collected in the presence of heparin. Then, 100 μL of plasma obtained by centrifugation (3500 rpm for 20 min) was diluted with 850 μL of saline and 50 μL of trichloroacetic acid was added to precipitate plasma proteins. The precipitated plasma proteins was removed by centrifuge (3000 rpm for 15 min) and 500 μL supernatant was diluted with 1.5 mL of saline and fluorescence was measured by fluorescence spectrophotometer at 270 nm excitation (corresponding to AHPP) and peak emission at 356.0 nm.

Results

Synthesis and characterizations of AHPP-PEG micelles

In the first method, mono-AHPP-PEG was synthesized using NOF PEG (ME-20 AS) which resulted in a water-soluble derivate of AHPP. In the second method, an

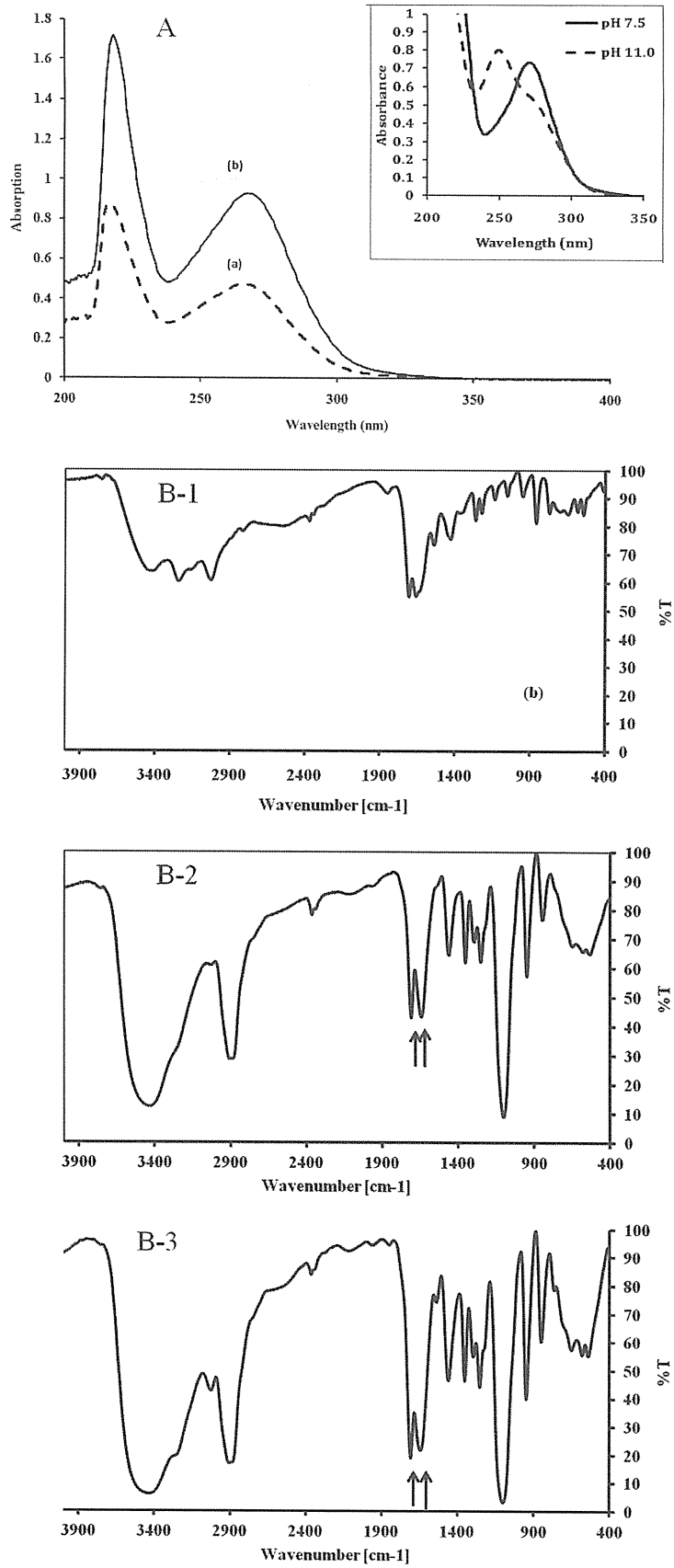

Figure 2. Characterization of AHPP-PEG micellar conjugates. (A) UV-vis spectroscopy of mono-AHPP-PEG (a) and bis-(AHPP)-PEG (b) in 0.025 M NaOH, concentrations used; 0.05 mg/mL. Inset image is for the UV absorption spectrum of AHPP. The λ_{max} for AHPP undergoes a bathochromic shift from 270 nm (pH 7.5) to 254.0 nm (pH 11.0). (B) FTIR spectrums of (B-1) AHPP; (B-2) mono-AHPP-PEG; and (B-3) bis-(AHPP)-PEG in KBr discs. The peak of AHPP becomes broader at 3400 cm^{-1} compared to AHPP-PEG due to large–NH stretching. The peak at about 1000 cm^{-1} is due to C-C stretching of PEG chain. The arrow indicates amide (B-2) and carbamate (B-3) peak.

activated PEG derivative was first synthesized employing PEG derivative of an active carbonate of *p*-nitorophenyl-chloroformate as described in Scheme 2. Both conjugates exhibited good water solubility up to 50 mg/mL (48 mM AHPP eqvt.), which is more than adequate concentration for dose escalation for clinical applications, and far greater than free AHPP (<0.05 mg/mL).

Characterization of AHPP-PEG conjugates

In both cases of AHPP-PEG conjugates, they were purified by Sephadex gel G-100 chromatography prior to their characterization by UV, IR spectroscopes. Figure 2A shows the UV-visible absorption spectra of mono-AHPP-PEG (a), and bis-(AHPP)-PEG (b), respectively. Free AHPP (Figure 2A, inset image) had a very strong absorption peak at 254 nm at higher pH 11.0, whereas at lower pH 7.5 the peak maxima shifted to 270 nm. The content of AHPP in the AHPP-PEG conjugates was calculated by specific UV absorption based on plotting a standard curve of free AHPP at pH 8.5 in 0.2 M phosphate buffer. In the elemental analysis, mono-AHPP-PEG conjugate showed a content of N, 2.84; C, 53.30; H, 8.51 and bis-(AHPP)-PEG conjugate showed N, 5.52; C, 52.39; H, 8.19; which is similar to the calculated value of N, 2.94; C, 53.50; H, 8.60 and N, 5.51; C, 52.90; H, 8.24 for mono-AHPP-PEG and bis-(AHPP)-PEG, respectively. As the PEG contains no nitrogen, the presence of nitrogen in AHPP-PEG micelles reflects the conjugation.

The extent of the reaction between primary amino groups of AHPP with activated PEG following the S_N2 type of reaction mechanism. Formation of AHPP-PEG conjugate between AHPP and PEG was confirmed by FTIR spectroscopy (Figure 2B). In FTIR spectrum, the N-H stretching of primary amine at 3350.0 cm^{-1} disappeared, and the peak at 1643.05 and 1708.6 cm^{-1} indicated the presence of–C=O groups, suggesting the conjugation of amine group of AHPP to the PEG.

Sephadex gel chromatography of AHPP-PEG conjugates

The calculated mean molecular weights based on chemical formula of PEG was mono-AHPP-PEG and

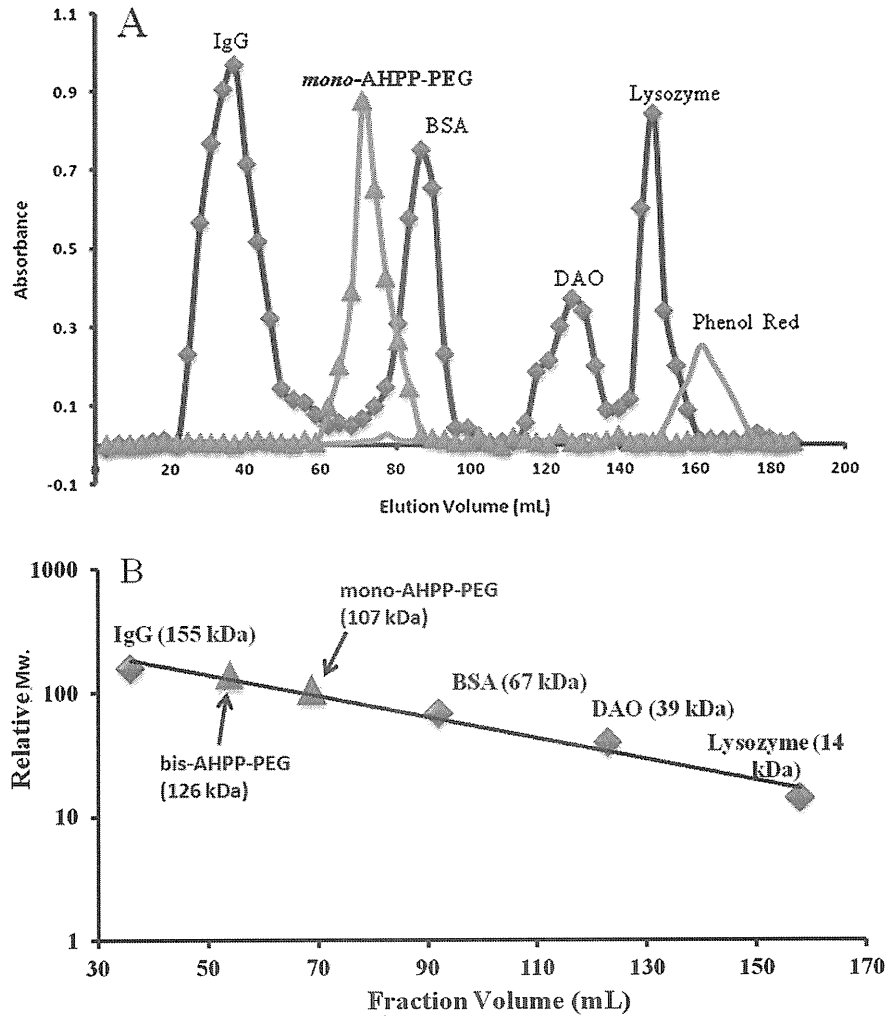

Figure 3. Sephadex G-100 purification and gel size exclusion chromatography of pegylated AHPP and standard proteins. (A) Standard proteins and AHPP-PEG conjugate. Detection wavelengths were 280.0 nm and 270.0 nm for standard proteins and AHPP-PEG conjugates, respectively. (B) Plot of relative molecular weight vs. fraction volume (mL) to determine the micellar size of AHPP-PEG conjugates.

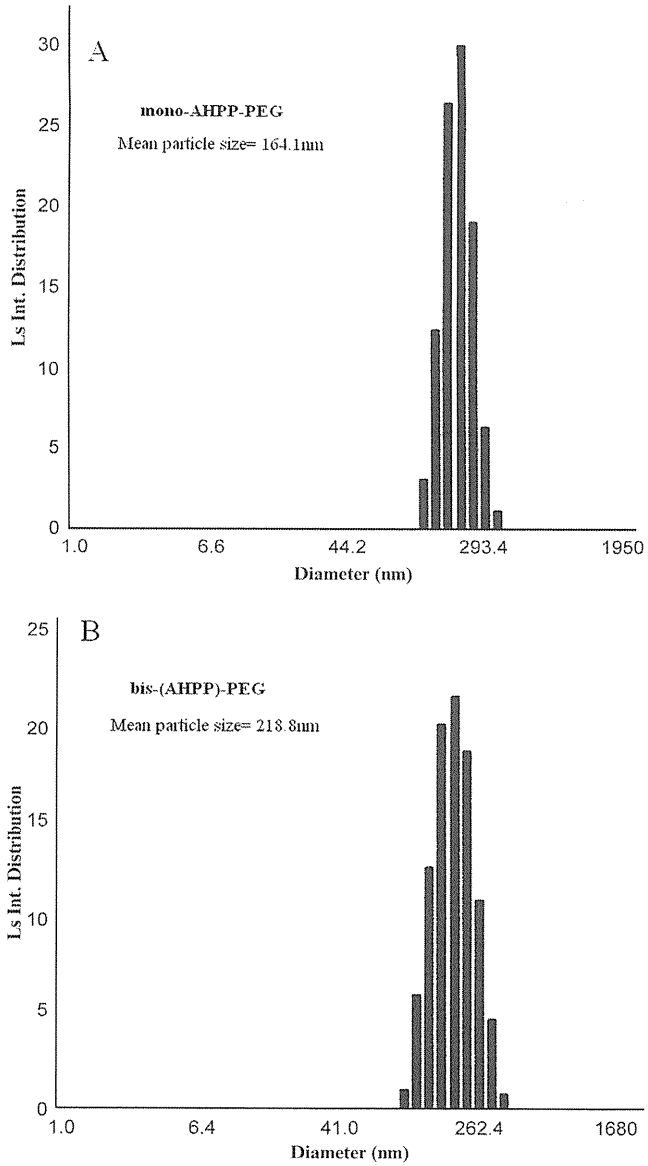

Figure 4. Dynamic light scattering (DLS) of pegylated AHPP micelles. The samples prepared in 0.15 M NaCl/0.01 M sodium phosphate buffer (pH 7.4). The average particle size of the micelles was 164.1 nm and 218.8 nm for (A) mono-AHPP-PEG and (B) bis-(AHPP)-PEG, respectively. Plot of Ls Int. Distribution vs. diameter was shown.

bis-(AHPP)-PEG conjugates are 2.2 and 2.3 kDa, respectively. However, Sephadex G-100 superfine (Amersham Biosciences AB, Uppsala, Sweden) high resolution gel chromatography showed a large apparent molecular sizes of 107 kDa and 126 kDa (Figure 3A), based on the standard proteins molecular weights markers [IgG, 155 kDa; bovine serum albumin (BSA), 67 kDa; lysozyme, 14 kDa] as shown in Figure 3B. These results indicates that, irrespective of the molecular size (2.2 kDa) of PEG chain, self-associate to form supramolecular assemblies in aqueous medium, similar to that reported earlier for several PEGylated micellar drugs and conjugates (Harada et al. 1999; Otsuka et al. 2003; Ideta et al. 2005; Veronese et al. 2005). The present result is also similar to that observed with the earlier preparation of polyethylene glycol–zinc protoporphyrin (PEG–ZnPP) and styrene-maleic acid copolymer-AHPP (SMA-AHPP) micelles in our laboratory using styrene-maleic acid (SMA) copolymer, where these conjugates shows large molecular size of about 116 kDa and 67 kDa, respectively, by Sephadex gel chromatography (Sahoo et al. 2002; Fang et al. 2009a). It is anticipated that these macromolecular conjugates are capable of utilizing the EPR effect for tumor selective delivery (Maeda et al. 2009b; Matsumera et al. 1886; Maeda et al. 2001c).

Solution behavior of the AHPP-PEG conjugates as analyzed by dynamic light scattering (DLS)

The micellar structure of the AHPP-PEG conjugates was further elaborated by DLS studies. The mono-AHPP-PEG and bis-(AHPP)-PEG micelles exhibited a mean particle size of 164.1 nm (Figure 4A) and 218.8 nm, respectively (Figure 4B). These are in line with the recently reported SMA-AHPP (Fang et al. 2009a) and PEG-ZnPP (Sahoo et al. 2002; Iyer et al. 2007b) micelles, which behave in a similar fashion forming self-assembled associations in aqueous solution. This result indicates that the micelles prepared by mono-AHPP-PEG conjugate have tighter interaction between PEG and AHPP resulting in smaller size of micelles than bis-(AHPP)-PEG. Moreover, there may be hydrophobic interaction among AHPP molecules as head group and PEG as hydrophilic tail (Nishide et al. 1977).

In addition, the results from gel chromatography showed a relatively smaller size than that of DLS. This is probably due to the interaction between AHPP-PEG and gel which resulting in a apparently smaller size, and it may thus not reflect the real size of AHPP-PEG micelle.

Quantification of amino group after conjugation with PEG

Loss of the primary amino group after reaction was quantified by two methods; (a) TNBS and (b) fluorescamine method. Degree of modification by TNBS was 87.47% and 91.2% for mono-AHPP-PEG and bis-(AHPP)-PEG conjugates respectively (Figure 5A). The fluorescamine assay results 88.22 and 93.98% for mono-AHPP-PEG and bis-(AHPP)-PEG conjugates respectively indicating most of the AHPP are reacted with polyethylene chains (Figure 5B).

Release of AHPP-PEG conjugate from the micelles

Because the AHPP-PEG is linked by covalent bond, free AHPP will not released in physiological condition. The release study is thus designed to investigate the release of AHPP-PEG conjugate from its micellar form. To support this notion, we found that no precipitation was observed both inside and outside the dialysis bag even after centrifugation because AHPP will precipitate in this condition if it is cleaved from AHPP-PEG. It is thus indicates that released AHPP is coupled with PEG.

As shown in Figure 6, very slow release rate was found in aqueous medium, about 1.1–1.2% per day for

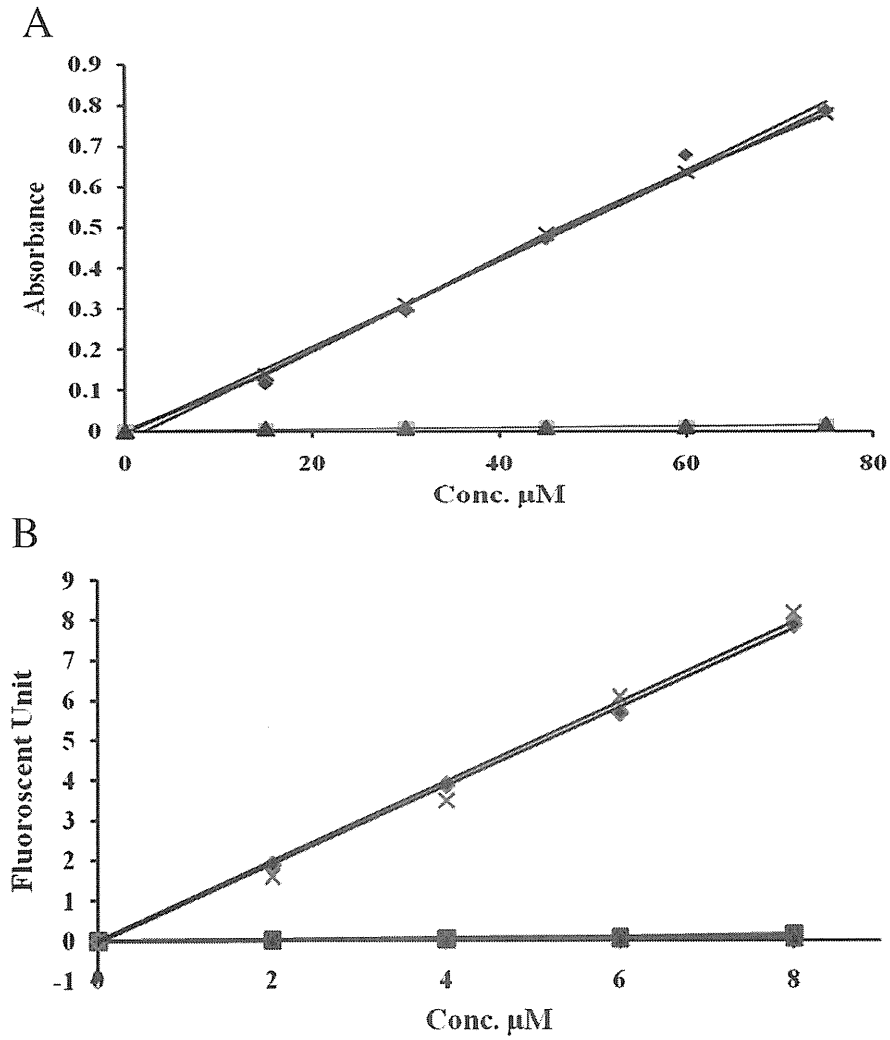

Figure 5. Quantification of amino groups and measurement of 3m Pegylation by (A) TNBS and (B) Fluoroscamine assay. (A) In TNBS assay absorbance was recorded at 355.0 nm corresponding to of λ_{max} of TNBS. (B) In fluorescamine assay sample solutions were excited at 390.0 nm was used and emission at 475.0 nm was measured corresponding to fluorescamine. Symbols: ♦ AHPP; X, mono-AHPP-PEG; ▲ bis-(AHPP)-PEG; ■ glycine.

the mono-AHPP-PEG (Figure 6A) and 1.5–1.6% per day for bis-(AHPP)-PEG (Figure 6B). Furthermore, the release below critical micellar concentration (CMC) level (0.3 mg/mL) was carried out and it was observed that below CMC level the release was fast i.e. almost 100% released within 3–4 h. Whereas, above CMC level the release was relatively slow i.e. 1.1–1.5%/day.

Stability studies of AHPP-PEG micelles

AHPP-PEG conjugates forms micelles in aqueous solutions, was further supported by a study using fluorescence spectroscopy. Namely, free AHPP in alkaline solution showed a strong fluorescence in 325–425 nm range upon excitation at 270.0 nm; however, when AHPP-PEG micelles dissolved in aqueous solutions, where it exists as densely packed form, the fluorescence of AHPP-PEG was almost quenched (Figure 7A) suggesting AHPP-PEG behaves as micellar structure, and the π–π interaction of AHPP quenches fluorescence due to energy transfer in the pack state as in micelle though in aqueous solution. Similar phenomena have been reported for the micellar drugs using SMA containing doxorubicin and pirarubicin in our previous work (Greish et al. 2004; Greish et al. 2005). Using fluorescence spectroscopy, we investigated the stability of AHPP-PEG micelles in various buffers with different pH 5.0–10.0. As shown in Figure 7B, the quenched states of fluorescence intensity of AHPP-PEG were observed over the range from pH 5.0 to 10.0, indicating the compact micellar structure is stable over a wide pH range.

The micellar stability and nature of AHPP-PEG conjugates in aqueous medium was further studied by fluorescence spectrophotometer and change of size of the micelles was monitored by DLS (figure 7C). When AHPP-PEG micelles were dissolved in distilled water or in neutral pHs up to pH 8.5 the integrity of micelles was conserved constant size at about 170 and 220 nm for mono-AHPP-PEG and bis-(AHPP)-PEG conjugates, respectively.

To study the stability of AHPP-PEG micelles under different pH conditions, or in presence of strong base, we

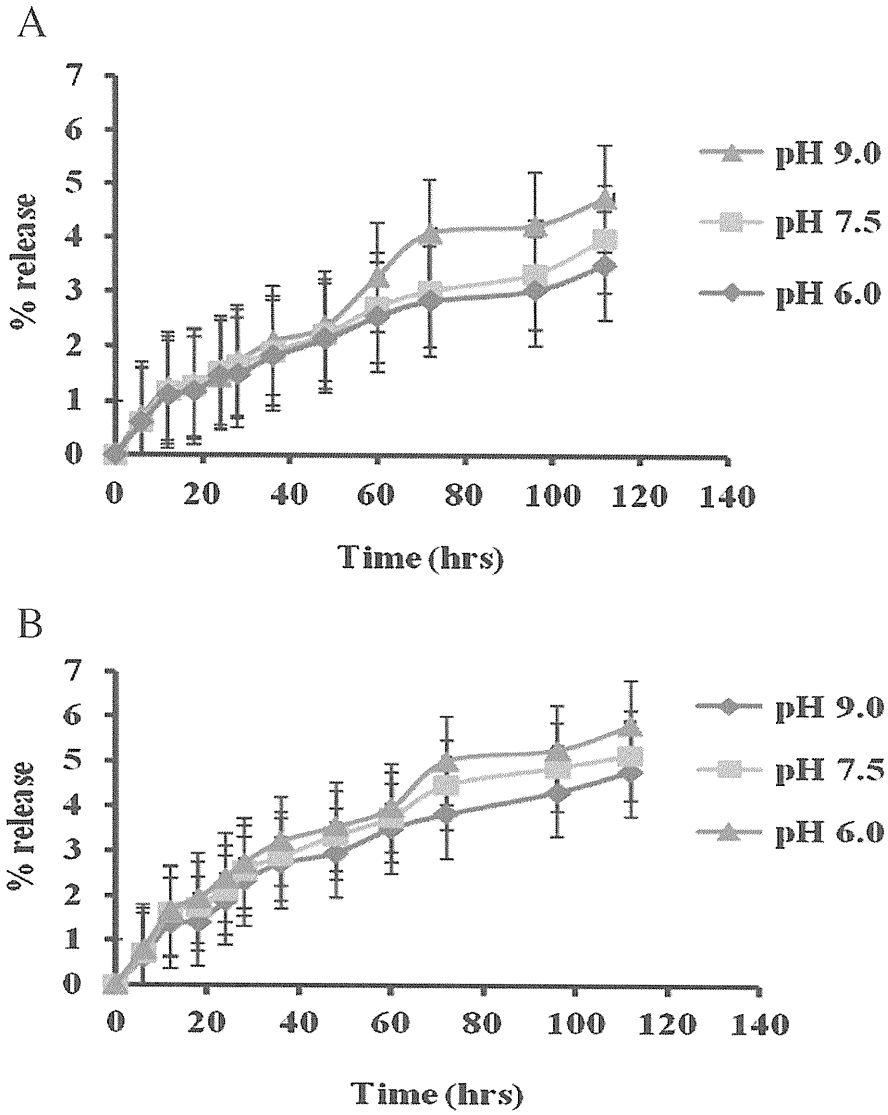

Figure 6. *In vitro* release from mono-AHPP-PEG (A) and bis-(AHPP)-PEG (B) conjugates. A constant release rate of ~1.2 and ~ 1.5% per day was observed at neutral pH for mono-AHPP-PEG and bis-(AHPP)-PEG, respectively. Release was quantified spectroscopically at 270.0 nm corresponding to AHPP was measured.

titrated the micellar solutions (1 mg/mL) against 0.1 M NaOH solutions, while monitoring the particle size by DLS and pH simultaneously (for details see Figure 7C). When 0.1 M NaOH was added drop wise into AHPP-PEG micellar solution (with increasing pH), it makes the micelles more and more unstable. At the end of titration, at pH 10.5 ± 0.1 units, the micellar size suddenly becomes very large ~1100 nm indicating the rupture or aggregation of micelle, corresponding to the inflection point in the curve (Figure 7). Both conjugates show similar stability and inflection point nearly at pH 10.5. Above the inflection point, we observed the disruption of micelles (burst effect), leading to an abrupt increase in the particle size.

Measurement of XO inhibitory activity by the AHPP-PEG conjugates

The initial velocity of uric acid formation was measured in the presence of various concentrations of xanthine and the XO inhibitors. Figure 8 shows the summary of the results of XO inhibition activity. AHPP inhibited XO in a competitive manner with an apparent inhibition constant Ki of 0.18 ± 0.02 μM, which was consistent with previous result (Fang et al. 2009a; Miyamoto et al. 1996). The apparent inhibitory constants (Ki) for mono-AHPP-PEG and bis-(AHPP)-PEG were estimated to be 0.23 ± 0.03 μM and 0.21 ± 0.03 μM, respectively. Both the AHPP conjugates show XO inhibition, which is comparable to native AHPP indicates AHPP-PEG conjugates itself is active towards XO. Similarly, PEGlylated AHPP conjugates may inhibit XO in a competitive manner.

In vivo pharmacokinetics of AHPP-PEG micelles

PEG-AHPP conjugates showed superior *in vivo* pharmacokinetics in ddY mice. The macromolecular micellar formulation of AHPP-PEG have relatively long circulation

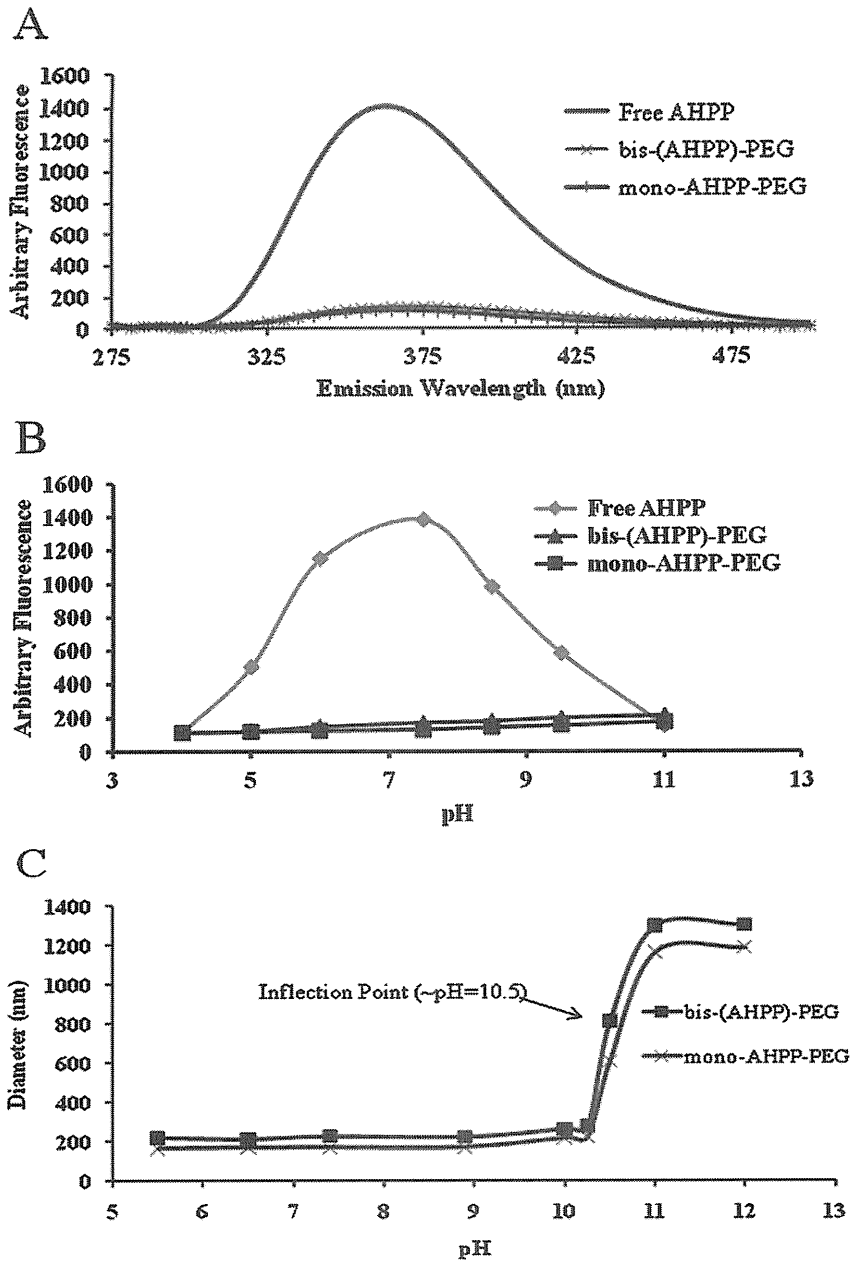

Figure 7. (A) Fluorescence spectra were recorded on F-2500 fluorospectrometer (Hitachi, Tokyo). The sample solutions were excited at 270.0 nm and emission from 275 to 500 nm was recorded, (B) The micellar stability of AHPP-PEG conjugates in different pH. The emission peak maxima (335.0 nm) were plotted against pH. (C) Micellar stability of conjugates (a) mono-AHPP-PEG and; (b) bis-(AHPP)-PEG was measured as a function of pH in various buffer solutions by DLS. Mostly micelles were nanoparticles (100–300 nm) in the range from pH 5.0 to pH 10.0 indicating their good stability in working pH range. Symbols: ■ mono-AHPP-PEG and ▲, bis-(AHPP)-PEG.

time: even 24 h after i.v. injection, about 35% remained in circulation, whereas more than 70% AHPP was cleared within 4 h after administration (Figure 9).

Discussion

In the present work, we synthesized PEG conjugated AHPP, which spontaneously formed micelles. Both conjugates showed potent XO inhibitory activity comparable to free AHPP and other polymer styrene-co-maleic acid copolymer (SMA) conjugated AHPP (Fang et al. 2009a). More importantly, the AHPP-PEG conjugates showed higher water solubility, which overcame the main drawback of native AHPP (which is practically water insoluble). The optimum AHPP content in the AHPP-PEG conjugates was about 7.5% for mono-AHPP-PEG and 15.1% for bis-(AHPP)-PEG, respectively.

Mean molecular weights of these conjugates of PEG-AHPP are about 2.2 and 2.3 kDa for mono-AHPP-PEG and bis-(AHPP)-PEG), respectively. However, Sephadex G-100 gel chromatography and DLS studies of AHPP-PEG conjugates indicated that they form supramolecular self-assembled association to form micellar structure in aqueous system; the critical micellar concentration

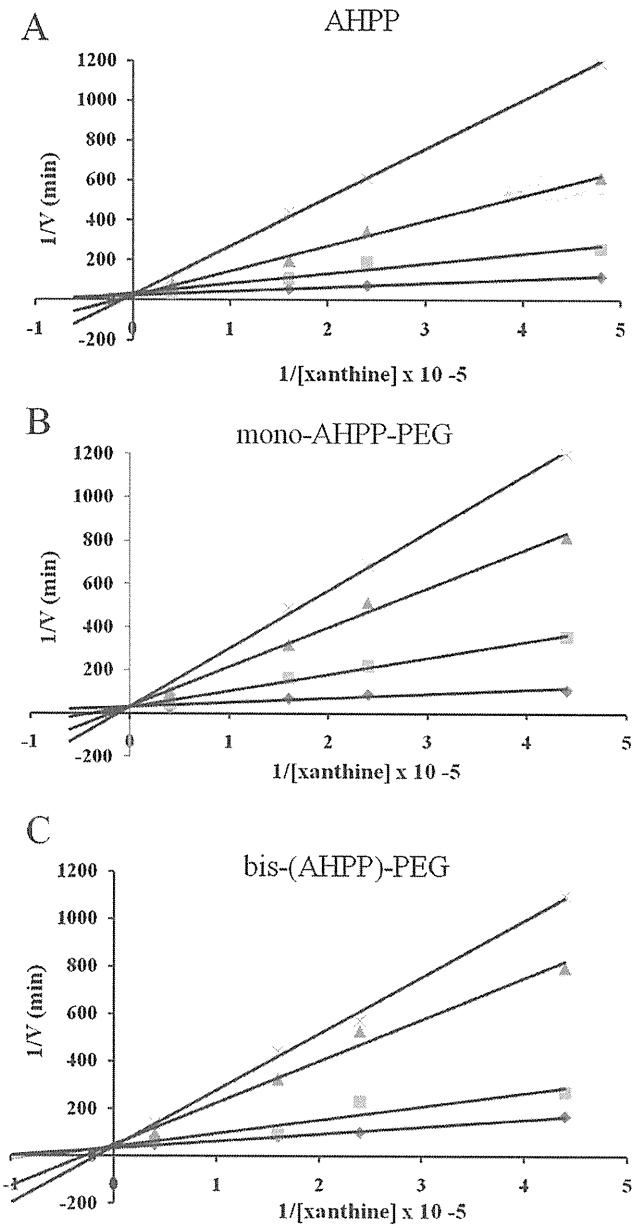

Figure 8. Lineweaver-Burk plot of PEG-AHPP conjugates for analysis of the XO inhibitory effects. (A) AHPP, (B) mono-AHPP-PEG and (C) bis-(AHPP)-PEG on the XO catalyze the oxidation of xanthine to uric acid. XO inhibitory activity of AHPP and AHPP-PEG conjugates was measured by measuring the rate of the uric acid formation in the presence of XO was determined spectrophotometrically. Concentrations and symbols for both conjugates used were: 0, ◆; 0.4, ■; 1.4, ▲; 2.4, and X, 4.4 μM. The apparent Ki values for AHPP, mono-AHPP-PEG and bis-(AHPP)-PEG were estimated to be 0.19 ± 0.03, 0.23 ± 0.03 μM and 0.21 ± 0.03 μM, respectively.

(CMC) of both AHPP-PEG conjugates was found to be about 0.3 mg/mL; therefore, above CMC level the AHPP-PEG conjugates will behave as macromolecule in blood circulation, thus exhibiting long plasma circulation time as evidenced by *in vivo* pharmacokinetics study (Figure 9). It is well known that biocompatible macromolecules show many beneficial characteristics such as prolonged

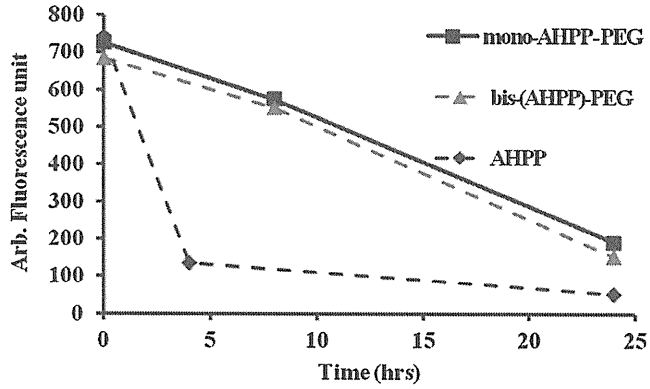

Figure 9. Pharmacokinetics of AHPP-PEG and native AHPP in blood of ddY mice. AHPP-PEG or native AHPP was injected i.v. into ddY mice via the tail vein. After scheduled intervals, mice were killed, blood was collected, and blood concentrations of AHPP and AHPP-PEG were measured as described in "methods". Values are means ± SE; $n = 3$.

in vivo half-life. For instance, the pyran copolymer-SOD derivatives synthesized in our laboratory showed prolonged plasma half-life of 6.0 h compared with ~4 min for the native SOD (Oda et al. 1989; Ogino et al. 1988). The result from this study (Figure 9) is in consistent to the previous reports. Furthermore, a PEGylated nanoscale polymeric carrier system provides stealth characteristics thereby prolonging plasma circulation time *in vivo* by avoiding uptake by reticuloendothelial system or phagocytic leukocytes (Sahoo et al. 2002; Greish et al. 2005).

The concept of macromolecular drugs is now widely applied in various clinical fields. For example, use of native interferon therapy has been almost replaced by PEG-interferon therapy (Iyer et al. 2006; Duncan et al. 2003; Vicent et al. 2006). PEG-ademase and PEG-aspargase are used for the severe combined immunodeficiency disease and leukemia respectively (Duncan et al. 2003). PEG is well accepted as safe drug carrier. Previously in our laboratory, pegylated anticancer agents like zinc protoporphyrin showed good tumor selectivity by taking advantage of EPR effect (Maeda et al. 2009a; Iyer et al. 2007a; Iyer et al. 2006). Thus, conjugates of AHPP-PEG not only resolves the problem of water-solubility, but it may take advantage of the pharmacokinetic merits because of its macromolecular micelle nature. Studies on cooperativity in the self-assembly of PEG-ZnPP, SMA-Pirarubicin, and SMA-ZnPP have been reported very recently (Sahoo et al. 2002; Iyer et al. 2007b; Greish et al. 2004; Fang et al. 2003). It was observed that AHPP-PEG micelles are more stable over the wide range of pH (5.0–10.0) probably because of strong interaction between AHPP head molecules, in the core of the micelles by forming hydrophobic associations.

The use of AHPP *in vivo* was first examined in spontaneous hypertensive rat (SHR model) for its antihypertensive effect (Miyamoto et al. 1996); wherein it was found that AHPP could reduced the blood pressure of SHR rat to ~70% of the initial blood pressure (Donald et al. 2009;

Miyamoto et al. 1996). It may thus be anticipated that the AHPP conjugated to PEG may improve the *in vivo* characteristics of the drug several folds, warranting further investigations.

Accordingly, from biological point of view, the principal objective of AHPP-PEG conjugation is to improve the pharmacokinetic drug profile. Along these lines AHPP-PEG conjugates may not only useful as an antihypertensive agent, but also may be beneficial for the treatment of ROS associated diseases such as heart diseases, prevention of $ONOO^-$ - mediated cytotoxicity and several others ROS related diseases. In addition, due to its macromolecular nature, AHPP-PEG conjugates may accumulate in the site of interest such as inflammation via the EPR effect (Maeda et al. 2001a), thus demonstrating its effect much selectively, whereas greatly decreases the potential side effects to the host.

In conclusion, we successfully synthesized AHPP-PEG conjugates by utilizing two different approaches. AHPP-PEG derivatives exhibit much improved water solubility and superior *in vivo* pharmacokinetics as well as potent XO inhibiting activity. As XO is the major cause of O_2^- in many diseases, we thus anticipate the application of AHPP-PEG conjugates for the treatment of ROS related diseases, which warrants further investigations.

Acknowledgments

We would like to acknowledge Prof. Toshihiro Nohara, Laboratory of Natural Medicine, Department of Pharmaceutical Sciences, Sojo University for discussion and suggestions regarding characterization.

Declaration of interest

This work was supported by Grants-in-Aid for Scientific Research on Cancer Priority Areas (20015045), Scientific Research (C) (20590049) and (S0801085) from the Ministry of Education, Culture, Sports, Science and Technology of Japan, and a grant from the Ministry of Health, Welfare and Labour (No. 23000001, H 23-3) 3rd Cancer Study Project of Japan, to H.M. Bharate G. Y. would like to thank Sojo University and BioDynamics Research Foundation, Japan, for a Fellowship to PhD studies. The authors declare no conflicts of interest.

References

Adachi T, Fukushima T, Usami Y, Hirano K. (1993). Binding of human xanthine oxidase to sulphated glycosaminoglycans on the endothelial-cell surface. Biochem J, 289 (Pt 2), 523–527.

Cappola TP, Kass DA, Nelson GS, Berger RD, Rosas GO, Kobeissi ZA, Marbán E, Hare JM. (2001). Allopurinol improves myocardial efficiency in patients with idiopathic dilated cardiomyopathy. Circulation, 104, 2407–2411.

Crow JP, Beckman JS. (1995). The role of peroxynitrite in nitric oxide-mediated toxicity. In: Koprowski H, Maeda H. (eds.). The Role of Nitric Oxide in Physiology and Pathophysiology. Current Topics in Microbiology and Immunology. Springer-Verlag, Berlin 196:57–73.

Donald LJ, Robert A, Mercedes C, Giovanni DS, Ferguson TB, Flegal K, Ford E, Furie K, Alan G, Greenlund K, Haase N, Hailpern S, Michael H, Howard V, Kissela B, Kittner S, Lackland D, Lisabet, L, Marelli A, McDermott M, Meigs J, Mozaffarian D, Nichol G, O'Donnell C, Roger V, Rosamond W, Sacco R, Sorlie P, Stafford R, Steinberger J, Thom T, Wasserthiel-Smoller S, Wong N, Wylie-Rosett J, Hong Y. (2009). Heart Disease and Stroke Statistics_2009. Update: A Report From the American Heart Association Statistics Committee and Stroke Statistics Subcommittee. Circulation 119:e21–e181.

Duncan R. (2003). The dawning era of polymer therapeutics. Nat Rev Drug Discov, 2, 347–360.

Fang J, Sawa T, Akaike T, Akuta T, Sahoo SK, Khaled G, Hamada A, Maeda H. (2003). *In vivo* antitumor activity of pegylated zinc protoporphyrin: targeted inhibition of heme oxygenase in solid tumor. Cancer Res, 63, 3567–3574.

Fang J, Iyer AK, Seki T, Nakamura H, Greish K, Maeda H. (2009a). SMA-copolymer conjugate of AHPP: a polymeric inhibitor of xanthine oxidase with potential antihypertensive effect. J Control Release, 135, 211–217.

Fang J, Seki T, Maeda H. (2009b). Therapeutic strategies by modulating oxygen stress in cancer and inflammation. Adv Drug Deliv Rev, 61, 290–302.

Feigelson P, Davidson JD, Robins RK. (1957). Pyrazolopyrimidines as inhibitors and substrates of xanthine oxidase. J Biol Chem, 226, 993–1000.

Freehold NJ. (1972). Xanthine Oxidase (milk). In: Worthington Enzyme Manual. Worthington Biochemical, pp. 30–31.

Greish K, Sawa T, Fang J, Akaike T, Maeda H. (2004). SMA-doxorubicin, a new polymeric micellar drug for effective targeting to solid tumours. J Control Release, 97, 219–230.

Greish K, Nagamitsu A, Fang J, Maeda H. (2005). Copoly(styrene-maleic acid)-pirarubicin micelles: high tumor-targeting efficiency with little toxicity. Bioconjug Chem, 16, 230–236.

Gryglewski RJ, Palmer RM, Moncada S. (1986). Superoxide anion is involved in the breakdown of endothelium-derived vascular relaxing factor. Nature, 320, 454–456.

Harada A, Kataoka K. (1999). Chain length recognition: core-shell supramolecular assembly from oppositely charged block copolymers. Science, 283, 65–67.

Huie RE, Padmaja S. (1993). The reaction of NO with superoxide. Free Radic Res Commun, 18, 195–199.

Ideta R, Tasaka F, Jang WD, Nishiyama N, Zhang GD, Harada A, Yanagi Y, Tamaki Y, Aida T, Kataoka K. (2005). Nanotechnology-based photodynamic therapy for neovascular disease using a supramolecular nanocarrier loaded with a dendritic photosensitizer. Nano Lett, 5, 2426–2431.

Iyer AK, Khaled G, Fang J, Maeda H. (2006). Exploiting the enhanced permeability and retention effect for tumor targeting. Drug Discov Today, 11, 812–818.

Iyer AK, Greish K, Seki T, Okazaki S, Fang J, Takeshita K, Maeda H. (2007a). Polymeric micelles of zinc protoporphyrin for tumor targeted delivery based on EPR effect and singlet oxygen generation. J Drug Target, 15, 496–506.

Iyer AK, Greish K, Fang J, Murakami R, Maeda H. (2007b). High-loading nanosized micelles of copoly(styrene-maleic acid)-zinc protoporphyrin for targeted delivery of a potent heme oxygenase inhibitor. Biomaterials, 28, 1871–1881.

Jarasch ED, Bruder G, Heid HW. (1986). Significance of xanthine oxidase in capillary endothelial cells. Acta Physiol Scand Suppl, 548, 39–46.

Jarasch ED, Grund C, Bruder G, Heid HW, Keenan TW, Franke WW. (1981). Localization of xanthine oxidase in mammary-gland epithelium and capillary endothelium. Cell, 25, 67–82.

Maeda H. (2001a). SMANCS and polymer-conjugated macromolecular drugs: advantages in cancer chemotherapy. Adv Drug Deliv Rev, 46, 169–185.

Maeda H. (2001b). The enhanced permeability and retention (EPR) effect in tumor vasculature: the key role of tumor-selective macromolecular drug targeting. Adv Enzyme Regul, 41, 189–207.

Maeda H, Sawa T, Konno T. (2001c). Mechanism of tumor-targeted delivery of macromolecular drugs, including the EPR effect in solid tumor and clinical overview of the prototype polymeric drug SMANCS. J Control Release, 74, 47–61.

Maeda H. (2009a). Controlling oxidative stress: therapeutic and delivery strategies. Preface. Adv Drug Deliv Rev, 61, 285–286.

Maeda H, Bharate GY, Daruwalla J. (2009b). Polymeric drugs for efficient tumor-targeted drug delivery based on EPR-effect. Eur J Pharm Biopharm, 71, 409–419.

Matsumura Y, Maeda H. (1986). A new concept for macromolecular therapeutics in cancer chemotherapy: mechanism of tumoritropic accumulation of proteins and the antitumor agent smancs. Cancer Res, 46, 6387–6392.

Miyamoto Y, Akaike T, Yoshida M, Goto S, Horie H, Maeda H. (1996). Potentiation of nitric oxide-mediated vasorelaxation by xanthine oxidase inhibitors. Proc Soc Exp Biol Med, 211, 366–373.

Moncada S, Palmer RM, Higgs EA. (1991). Nitric oxide: physiology, pathophysiology, and pharmacology. Pharmacol Rev, 43, 109–142.

Nishide H, Mihayashi K, Tsuchida E. (1977). Dissociation of aggregated ferroheme complexes and protoporphyrin IX by water-soluble polymers. Biochim Biophys Acta, 498, 208–214.

Oates JA, Brown NJ. (2001). Antihypertensive agents and the drug therapy of hypertension. In: Hardman JG, Limbird LE, Gilman AG, (eds.).Goodman & Gilman's the pharmacological basis of therapeutics (10th Edition), The McGraw-Hill Companies, Inc., New York. pp. 871–896.

Oda T, Akaike T, Hamamoto T, Suzuki F, Hirano T, Maeda H. (1989). Oxygen radicals in influenza-induced pathogenesis and treatment with pyran polymer-conjugated SOD. Science, 244, 974–976.

Ogino T, Inoue M, Ando Y, Awai M, Maeda H, Morino Y. (1988). Chemical modification of superoxide dismutase. Extension of plasma half life of the enzyme through its reversible binding to the circulating albumin. Int J Pept Protein Res, 32, 153–159.

Otsuka H, Nagasaki Y, Kataoka K. (2003). PEGylated nanoparticles for biological and pharmaceutical applications. Adv Drug Deliv Rev, 55, 403–419.

Pacher P, Nivorozhkin A, Szabó C. (2006). Therapeutic effects of xanthine oxidase inhibitors: renaissance half a century after the discovery of allopurinol. Pharmacol Rev, 58, 87–114.

Radi R, Beckman JS, Bush KM, Freeman BA. (1991). Peroxynitrite oxidation of sulfhydryls. The cytotoxic potential of superoxide and nitric oxide. J Biol Chem, 266, 4244–4250.

Sahoo SK, Sawa T, Fang J, Tanaka S, Miyamoto Y, Akaike T, Maeda H. (2002). Pegylated zinc protoporphyrin: a water-soluble heme oxygenase inhibitor with tumor-targeting capacity. Bioconjug Chem, 13, 1031–1038.

Stocks SJ, Jones AJ, Ramey CW, Brooks DE. (1986). A fluorometric assay of the degree of modification of protein primary amines with polyethylene glycol. Anal Biochem, 154, 232–234.

Veronese FM, Largajolli R, Boccù E, Benassi CA, Schiavon O. (1985). Surface modification of proteins. Activation of monomethoxy-polyethylene glycols by phenylchloroformates and modification of ribonuclease and superoxide dismutase. Appl Biochem Biotechnol, 11, 141–152.

Veronese FM, Schiavon O, Pasut G, Mendichi R, Andersson L, Tsirk A, Ford J, Wu G, Kneller S, Davies J, Duncan R. (2005). PEG-doxorubicin conjugates: influence of polymer structure on drug release, *in vitro* cytotoxicity, biodistribution, and antitumor activity. Bioconjug Chem, 16, 775–784.

Vicent MJ, Duncan R. (2006). Polymer conjugates: nanosized medicines for treating cancer. Trends Biotechnol, 24, 39–47.

International Journal of Pharmaceutics 420 (2011) 111–117

Contents lists available at ScienceDirect

International Journal of Pharmaceutics

journal homepage: www.elsevier.com/locate/ijpharm

Pharmaceutical Nanotechnology

Synthesis and evaluation of poly(styrene-*co*-maleic acid) micellar nanocarriers for the delivery of tanespimycin

Nate Larson[a,b], Khaled Greish[a,b,*,1], Hillevi Bauer[a,b], Hiroshi Maeda[d], Hamidreza Ghandehari[a,b,c,**]

[a] *Department of Pharmaceutics and Pharmaceutical Chemistry, Salt Lake City, UT 84108, USA*
[b] *Center for Nanomedicine, Nano Institute of Utah, Salt Lake City, UT 84108, USA*
[c] *Department of Bioengineering, University of Utah, Salt Lake City, UT 84108, USA*
[d] *Research Institution of DDS, Sojo University, Kumamoto 860-0082, Japan*

ARTICLE INFO

Article history:
Received 9 May 2011
Received in revised form 28 July 2011
Accepted 8 August 2011
Available online 12 August 2011

Keywords:
Tanespimycin
17-AAG
Polymeric micelle
Prostate cancer

ABSTRACT

Polymeric micelles carrying the heat shock protein 90 inhibitor tanespimycin (17-*N*-allylamino-17-demethoxygeldanamycin) were synthesized using poly(styrene-*co*-maleic acid) (SMA) copolymers and evaluated *in vitro* and *in vivo*. SMA-tanespimycin micelles were prepared with a loading efficiency of 93%. The micelles incorporated 25.6% tanespimycin by weight, exhibited a mean diameter of 74 ± 7 nm by dynamic light scattering and a zeta potential of −35 ± 3 mV. Tanespimycin was released from the micelles in a controlled manner *in vitro*, with 62% released in 24 h from a pH 7.4 buffer containing bovine serum albumin. The micellar drug delivery systems for tanespimycin showed potent activity against DU145 human prostate cancer cells, with an IC_{50} of 230 nM. They further exhibited potent anti-cancer activity *in vivo* in nu/nu mice bearing subcutaneous DU145 human prostate cancer tumor xenografts, with significantly higher anticancer efficacy as measured by tumor regression when compared to free tanespimycin at an equivalent single dose of 10 mg/kg. These data suggest further investigation of SMA-tanespimycin as a promising agent in the treatment of prostate cancer.

1. Introduction

Heat shock protein 90 (Hsp90) is a 90 kDa chaperone protein that facilitates the cellular response to stress by regulating the folding and activity of many client proteins, which include critical growth-stimulating proteins involved in the malignant transformation of various cancers (Sharp and Workman, 2006). Hsp90 expression is elevated during cellular stress conditions such as heat, pH, and glucose deprivation (Buchner, 1999) and in a variety of cancers including melanoma, leukemia, colon, lung, breast, and prostate (Fukuyo et al., 2010).

Geldanamycin (GDM), a benzoquinone ansamycin derived from *Streptomyces hygrocopicus*, is a naturally occurring inhibitor of Hsp90 and has been studied extensively as an anticancer agent (Porter et al., 2009). GDM binds to the N-terminal ATP-binding site of Hsp90 and induces degradation of its client proteins (Whitesell and Lindquist, 2005). This ability of GDM to alter multiple oncogenic pathways makes GDM an attractive therapeutic compound. However, the clinical use of GDM has been limited by multiple factors. It exhibits high hepatotoxicity at therapeutic doses in animal models (Supko et al., 1994), is poorly soluble in water, and is metabolically unstable (Fukuyo et al., 2010). A GDM derivative 17-*N*-allylamino-17-demethoxygeldanamycin (tanespimycin, 17-AAG) has been widely investigated as an alternative to GDM, and has shown less toxicity and comparable activity compared to GDM in mouse models (Kelland et al., 1999; Burger et al., 2004). This drug was the first-in-class Hsp90 inhibitor to enter clinical trials (Banerji et al., 2005). Although the therapeutic index for tanespimycin is increased as compared to GDM, dose limiting toxicity is still due to hepatic and gastrointestinal symptoms (Sausville et al., 2003). Delivery of tanespimycin is difficult due a poor aqueous solubility of 0.02–0.05 mg/mL (Ge et al., 2006), requiring the use of surfactants such as Cremophor® EL, which are known to induce histamine release, resulting in hypersensitivity reactions and anaphylaxis (Rowinsky and Donehower, 1995), and are further associated with hyperlipidaemia, abnormal lipoprotein patters, aggregation of erythrocytes, and peripheral neuropathy (Gelderblom et al., 2001).

* Corresponding author at: Department of Pharmaceutics and Pharmaceutical Chemistry, University of Utah, 383 Colorow Road, Room 339, Salt Lake City, UT 84108, USA. Tel.: +1 801 587 1558.
** Corresponding author at: Department of Pharmaceutics and Pharmaceutical Chemistry and Bioengineering, University of Utah, 383 Colorow Road, Room 343, Salt Lake City, UT 84108, USA. Tel.: +1 801 587 1566.
E-mail addresses: khaled.gerish@utah.edu, khaled.gerish@otago.ac.nz (K. Greish), hamid.ghandehari@pharm.utah.edu (H. Ghandehari).
[1] *Present address*: Department of Pharmacology & Toxicology, Otago School of Medical Sciences, University of Otago, Dunedin, New Zealand, Tel.: + 64 3 479 4095; + 64 21 310 335.

0378-5173/$ – see front matter © 2011 Elsevier B.V. All rights reserved.
doi:10.1016/j.ijpharm.2011.08.011

Polymeric carriers can increase the solubility of poorly water soluble drugs and can accumulate in tumor tissues via the "enhanced permeability and retention" (EPR) effect (Matsumura et al., 1987; Greish et al., 2003), thereby increasing the therapeutic index for a given chemotherapeutic agent. Polymeric micelles are characterized by a hydrophilic shell which interacts with an external aqueous environment and a hydrophobic core which acts as a depot for hydrophobic drugs. Polymeric micelles were first reported as potential carriers for use in cancer treatment in the early 1980s (Gros et al., 1981) and the field has matured to include a number of candidates currently under clinical investigation (Blanco et al., 2009).

The use of poly(styrene-*co*-maleic acid) (SMA) micelles as drug carriers is currently under investigation (Iyer et al., 2007; Daruwalla et al., 2010). SMA has been proven to be biologically safe and is used clinically in SMANCS, a conjugate of half-butyl SMA bound to the antitumor protein neocarzinostatin (Maeda, 2001). Previous studies have demonstrated immunopotentiating activity associated with SMA moieties, in contrast to immunosuppression that is typically induced by conventional chemotherapeutics (Suzuki et al., 1988, 1990). The styrenic core of SMA micelles has been characterized by a high glass transition temperature (Rodriguez et al., 2008) and a large microviscosity (Claracq et al., 2002), which may help facilitate higher stability and more controlled release rates of drugs from the micelle core. In addition, the hydrophilic surface of SMA micelles is comprised of carboxyl terminated maleic acid groups, allowing easy surface modification or conjugation with targeting moieties.

Previous work by our group (Borgman et al., 2009; Larson et al., 2010) and others (Kasuya et al., 2002) has described the use of HPMA copolymers as drug carriers for geldanamycin derivatives. In these systems, geldanamycin derivatives are covalently bound to the polymer backbone via the lysosomally degradable Gly-Phe-Leu-Gly linker (Subr et al., 1988), resulting in highly stable conjugates with drug release occurring via lysosomal degradation following endocytosis. The use of such systems however requires chemical modification of geldanamycin to facilitate conjugation, and such modifications result in a decrease in the activity of geldanamycin. Self-assembled drug delivery systems do not suffer from this limitation as the drug is most often bound to the carrier through non-covalent hydrophobic interactions.

In the present study, SMA was used to prepare polymeric micelles containing the Hsp90 inhibitor tanespimycin. The micelles were characterized for drug loading efficiency, drug content, size, and zeta potential. The release rate of tanespimycin from the micelles and the ability of the micelles to inhibit the growth of DU145 human prostate cancer cells *in vitro* were evaluated. An *in vivo* preliminary single dose study evaluating the efficacy of the micelles was performed in nu/nu mice bearing DU145 human prostate cancer xenografts.

2. Materials and methods

2.1. Materials

Geldanamycin (NSC 122750) was kindly supplied by the National Cancer Institute Developmental Therapeutics Program (NCI DTP). Allylamine was supplied by Alfa Aesar (Ward Hill, MA, USA). Cumene terminated poly(styrene-*co*-maleic anhydride) was obtained from Sigma–Aldrich Corp. (St. Louis, MO, USA) and supplied with a 1.3:1 mole ratio of styrene:maleic anhydride, an average M_n of approximately 1600 as determined by GPC, and an acid number of 465–495 mg KOH/g. *N*-(3-Dimethylaminopropyl)-*N'*-ethylcarbodiimide hydrochloride (EDAC) was obtained from Sigma–Aldrich Corp. Bovine serum albumin (BSA) fraction V was obtained from MP Biomedicals (Solon, OH, USA). Polyoxyl castor oil (Cremophor® EL) was obtained from BASF Corp. (Florham Park, NJ, USA). Poly(ethylene glycol) 400 was obtained from Dow Chemical Corp. (Petaluma, CA, USA).

2.2. Cell lines and culture

The human prostate cancer cell line DU145 (ATCC, Rockville, MD, USA) was maintained in Eagle's minimum essential medium (ATCC) supplemented with 10% heat inactivated fetal bovine serum. Cell lines were cultured at 37 °C in a humidified atmosphere of 5% CO_2. For all procedures, cells were harvested using TrypLE™ Express (Invitrogen, Carlsbad, CA) and cell lines were maintained in a logarithmic growth phase during all studies.

2.3. Synthesis of tanespimycin

200 mg (0.357 mmol) of GDM was dissolved in 10 mL anhydrous dimethylformamide (DMF) at ambient temperature. 80.1 μL (1.07 mmol) of allylamine was added and the solution was kept under nitrogen, protected from exposure to light, and allowed to stir overnight at ambient temperature. The color of the solution changed from bright yellow-orange to dark purple and completion of the reaction was monitored by TLC on silica gel with chloroform:MeOH [9:1] as mobile phase by the disappearance of GDM. DMF was removed by rotary evaporator, and the resulting crude product was recrystallized from H_2O:EtOH [4:1]. The precipitate was analyzed by electrospray ionization mass spectrometry (ESI-MS).

2.4. Preparation of SMA-tanespimycin

Preparation of SMA micelles was similar to the method previously reported with modifications (Greish et al., 2004). First, poly(styrene-*co*-maleic anhydride) was hydrolyzed under aqueous alkaline conditions. Deionized water was adjusted to pH 14 with 4 N NaOH and heated to 70 °C. Poly(styrene-*co*-maleic anhydride) was added under stirring and the solution was maintained at pH 14 and 70 °C. The resulting hydrolyzed SMA solution was adjusted to pH 7.0 with 1 N HCl, diluted to a final concentration of 50 mg/mL, and allowed to cool to ambient temperature. 12 mL (600 mg SMA) was removed and diluted to approximately 60 mL with deionized water. 200 mg of tanespimycin was dissolved in minimal DMSO, and added drop wise while stirring, resulting in a cloudy solution. The solution was then adjusted to a pH of 5.0 and 600 mg EDAC in 5 mL deionized water was added drop wise at pH 5.0 and allowed to stir for 30 min. Next, the solution was adjusted to pH 10.5 by the addition of 1 N NaOH, the pH was subsequently adjusted to 7.0 with 1 N HCl, and the resulting solution was filtered to remove undissolved tanespimycin. 1 N HCl was then added dropwise to the filtrate to precipitate the micelles. The precipitated micelles were then centrifuged and purified by washing repeatedly with cold 0.01 N HCl in deionized water. Residual water/HCl was removed by lyophilization to obtain the final SMA-tanespimycin product.

2.5. Loading efficiency of SMA-tanespimycin

For the purpose of this study, loading efficiency is defined as the total weight of the drug in the final SMA-tanespimycin product divided by the initial weight of the drug introduced for micellar preparation. A standard curve was prepared by serial dilution of tanespimycin in DMSO and quantification of the drug was by UV spectrometry at 335 nm. Loading efficiency and drug content were then obtained by dissolving SMA-tanespimycin in DMSO and measuring absorbance at 335 nm in comparison with the standard curve.

To ensure that the drug was unmodified during micelle preparation, SMA-tanespimycin was further analyzed by reversed phase high-performance liquid chromatography (RP-HPLC). Analysis was performed with an Agilent 1100 LC system equipped with an Alltech Alltima C18 5 μm 150 × 4.6 mm column and a photo diode array detector scanning at 200–500 nm. The mobile phase consisted of deionized water and acetonitrile (ACN), at the following gradient: analysis time 0 min, 35% ACN; 15 min, 65% ACN; 25 min, 75% ACN; 30 min 95% ACN; 39 min, 100% ACN; 40 min, 65% ACN. A post time of 5 min was used to allow column equilibration between samples. The flow rate was maintained at 1.0 mL/min throughout and the sample injection volume was 20 μL. Samples of tanespimycin and SMA-tanespimycin were prepared in deionized water:ACN [65:35] and injected for analysis. The λ_{max} of tanespimycin at 335 nm was used for final quantitative analysis.

2.6. Size and zeta potential of SMA-tanespimycin

SMA-tanespimycin was prepared in 50 mM sodium phosphate buffer pH 7.4 at a concentration of 1.0 mg/mL for analysis. All measurements were performed at 25 °C. A Malvern Zeta Sizer ZEN3600 (Malvern Instruments Inc., Westborough, MA) was used to determine mean *Z*-average size, size distribution and zeta-potential. All measurements were performed on three separately prepared samples.

2.7. Drug release from SMA-tanespimycin

The release of tanespimycin from the micellar preparations was evaluated using a dialysis method and compared to the release in a standard vehicle formulation of EtOH:Cremophor® EL:PEG 400 [2:1:1] (EtOH:CrEL:PEG) (Zhong and Licari, 2005). SMA-tanespimycin was prepared at a concentration of 2.5 mg/mL (0.625 mg/mL tanespimycin) and drug-EtOH:CrEL:PEG was prepared by dissolving tanespimycin in EtOH:CrEL:PEG followed by a 10× dilution to yield a final concentration of 0.625 mg/mL. Samples were prepared in a 50 mM sodium phosphate buffer pH 7.4 or phosphate buffered saline (PBS) pH 7.4 with 40 mg/mL BSA. 4 mL of each sample was placed in a dialysis tube with a molecular weight cutoff of 3500 Da and dialyzed against 5 L of either 50 mM sodium phosphate buffer pH 7.4 or PBS pH 7.4. Media outside the dialysis membrane was changed periodically to ensure a constant sink condition. At each predetermined time point, 200 μL of the sample inside the dialysis membrane was removed and analyzed spectrophotometrically at 335 nm. Quantification of percent release was performed by comparison of sample absorbance with calibration curves prepared for SMA-tanespimycin and tanespimycin-EtOH-CrEL:PEG for each test condition. All experiments were performed in triplicate. Percent release is reported as mean ± standard deviation.

2.8. In vitro growth inhibition against human prostate cancer cells

The ability of the SMA-tanespimycin to inhibit the growth of DU145 human prostate cancer cells was evaluated using a 2-(2-methoxy-4-nitrophenyl)-3-(4-nitrophenyl)-5-(2,4-disulfophenyl)-2H-tetrazolium,monosodium salt (WST-8) cell viability assay. 3000 DU145 cells per well were plated in 96-well plates for 24 h. Cell culture medium was then removed and cells were treated with SMA-tanespimycin, tanespimycin dissolved in EtOH:CrEL:PEG, or controls for 72 h. Following treatment, medium was removed and wells were washed with 200 μL PBS. 100 μL of 10% (v/v) WST-8 reagent in complete growth medium was added to each well, cells were incubated at 37 °C/5% CO_2 for 120 min and absorbance at 450 nm minus 630 nm was determined by UV spectrophotometry. Relative viability was calculated by normalization of the absorbance of untreated cells. All experiments were performed in triplicate, with $n = 3$ wells per replicate. Non-linear least-squares regression analysis and calculation of IC_{50} was performed using GraphPad Prism.

2.9. In vivo efficacy

Six-week-old athymic (*nu/nu*) mice were obtained from Charles River Laboratories (Davis, CA, USA) and used in accordance with the Institutional Animal Care and Use Committee (IACUC) of the University of Utah. Mice were anesthetized using 4% isoflurane mixed with oxygen followed by subcutaneous injection of 1×10^7 DU145 cells per flank ($n = 5$ mice per treatment group). When the mean tumor size had reached approximately 50 mm^3 (about 10 days after tumor inoculation), the mice were treated with a single injection of either saline (control), free tanespimycin dissolved in DMSO, or SMA-tanespimycin at a dose of 10 mg/kg drug equivalent. The animals were routinely monitored and tumor growth was measured twice weekly and tumor volume was calculated as length × width^2 × $\pi/6$. Tumor volumes at each time point were normalized by the initial tumor volume and are reported as mean ± standard error of the mean. Animal weights were also measured at each time point and normalized to initial weight reported as mean ± standard deviation.

2.10. Statistical analysis

For release studies, tumor regression, and animal weight data, differences between data sets were determined by two-way repeated measures ANOVA using GraphPad Prism. Where differences were detected, a Bonferroni post-test was used to test for significance between groups. The significance level was set to $\alpha = 0.05$ for all statistical tests.

3. Results and discussion

3.1. Synthesis and preparation of SMA-tanespimycin

The development of polymeric micelles in drug delivery has primarily focused on the use of amphiphilic block copolymers with poly(ethylene glycol) (PEG) as the hydrophilic segment and a polyester or a poly(amino acid) derivative as the hydrophobic segment (Croy and Kwon, 2006). The loading of hydrophobic drugs and the assembly of such copolymers into micellar structures is commonly performed using methods such as: (1) basic equilibration, (2) dialysis, (3) oil/water emulsion, (4) solution casting, or (5) freeze drying (Gaucher et al., 2005). The present study describes polymeric micelles prepared by varying the pH of an aqueous solution containing poly(styrene-*co*-maleic acid) copolymers and tanespimycin, as a hydrophobic drug.

Tanespimycin was synthesized from GDM, and the resulting purple solid was collected and identified as tanespimycin by ESI-MS. SMA-tanespimycin was prepared by varying the pH of an aqueous solution of hydrolyzed SMA (Fig. 1).

3.2. Characterization of SMA-tanespimycin

The preparation of polymeric micelles as drug carriers often employ methods that result in either low loading efficiency or low drug loading capacity (Park, 2007). Using the aforementioned process, hydrolyzed SMA incorporated tanespimycin with a loading efficiency of 93% (Table 1), a significant improvement over previous studies describing polymeric micellar formulations of tanespimycin (Xiong et al., 2009; Shin et al., 2009).